1970

The influence of a carbon ablation layer on radiation from a hydrogen shock layer

Birbal Singh

Department:

THE INFLUENCE OF A CARBON ABLATION LAYER ON RADIATION FROM A HYDROGEN SHOCK LAYER

by

BIRBAL SINGH - 1943

A

THESIS

submitted to the faculty of

THE UNIVERSITY OF MISSOURI - ROLLA

in partial fulfillment of the requirements for the

Degree of

MASTER OF SCIENCE IN MECHANICAL ENGINEERING

Rolla, Missouri

1970

Approved by

H. F. Nelson (advisor) A. L. Crosbie

Xavier DR Avula

ABSTRACT

The effect of ablation heat shields on the radiative heat transfer to vehicles entering hydrogen atmospheres at thermo-dynamic conditions similar to those expected in Jovian atmospheres is investigated. The shock layer is assumed to consist of two plane parallel layers, one consisting of pure hydrogen species, and the other consisting of carbon species only. Each layer is assumed to be in local thermodynamic equilibrium at its respective temperature. The thermodynamic conditions in the hydrogen layer are arrived at by solving the Rankine-Hugoniot Equations across the shock. The temperature of carbon layer is taken as (3000, 5000, and 7000^{o}K) to cover the range of possible surface temperatures. Two entry velocities (115,000 and 190,000 fps) and four ambient densities (10^{-6} through 10^{-9} gm/cm^{3}) are considered. Four ratios of carbon layer thickness to total shock layer thickness (0.0, 0.05, 0.10, and 0.15) are considered, and the total shock layer thickness is allowed to vary from 0.1 to 10 cm. Both line (including carbon bands) and continuum processes are considered. The results show that:

1) The carbon layer reduces the flux reaching the surface from hydrogen layer in most cases, but not always. The reduction increases as the density and velocity increase. The ablation layer

increases the flux when the hydrogen layer is optically thin and the ablation layer is optically thick.

2) Atomic carbon is the most effective absorber in the carbon layer. Molecular carbon bands also become important as the ambient density and temperature decrease.

3) The atomic and ionic carbon lines are unimportant in reducing or increasing the flux from the hydrogen layer. This is because the half-widths of these lines are small and the population of ionic carbon is not large at the temperature considered in the study.

An error was detected in the computer program for the calculation of the position of the hydrogen edges. Two cases with correct positions of the hydrogen edges were run on the computer and the corrected results are shown in Appendix E. The numerical value of continuum flux changed considerably, but the trends of the results appear to be similiar to those discussed in the body of the thesis. Further results were not computed due to the expense of the computer runs.

TABLE OF CONTENTS

ACKNOWLEDGEMENTS

The author wishes to express his sincere appreciation to Dr. H.F. Nelson for his guidance and advice in the preparation of this thesis.

Appreciation is extended to Dr. A.L. Crosbie for his critical review of this thesis and constructive comments.

LIST OF FIGURES

LIST OF FIGURES (Continued)

LIST OF TABLES

LIST OF TABLES (Continued)

NOMENCLATURE

A	=	Avagadro's number.
$B_\nu(t)$	=	Planck function.
$b(\nu)$	=	line shape (sec).
c	=	velocity of light (2.99793×10^{10} cm/sec).
e	=	electronic charge (4.80286×10^{-10} statcouloumb).
$F(\lambda,T)$	=	emission coefficient.
F	=	flux (erg/cm^2 sec).
$f_{\ell u}$	=	f- number for the transition $\ell \rightarrow u$.
g_{bf}	=	bound-free Gaunt factor.
g_{ff}	=	free-free Gaunt factor.
g_n	=	statistical weight of quantum state n.
h	=	Planck's constant (6.6251×10^{-27} erg-sec).
i	=	enthalpy (ergs/gram).
I	=	intensity of radiation (erg/(cm^{2}sr)).
I_i	=	ionization potential of species i (ev).
k	=	Boltzmann's constant ($1.3804 \times 1_0^{-16}$erg/^{o}K).
k'_ν	=	effective absorption coefficient of species (cm^{-1}).
L_1	=	thickness of hydrogen layer.
L_2	=	thickness of carbon layer.
ℓ	=	lower state of bound-bounnd transition.
N_n	=	number density of the N^{th} quantum level (cm^{-3}).
H'_H	=	initial number density of hydrogen type species.
P_e	=	electron pressure (dynes/cm^2).

NOMENCLATURE (Continued)

P	=	pressure (atmospheres).
Q_i	=	electronic partition function of specie i.
R_H	=	Tydberg constant for hydrogen (109677.581 cm^{-1})
T	=	temperature ^oK.
V	=	velocity (ft/sec).
Z	=	partition function.
γ_{Lu}	=	electron impact half-width (1/sec).
λ	=	wavelength (Angstroms).
λ_0	=	unperturbed wave lengths (Angstroms).
ν	=	frequency (1/sec).
$\nu_{\ell u}$	=	frequency of transition $\ell \rightarrow u$ (1/sec).
ρ	=	density (gram/cm^3).
ρ_D	=	Debye radius (em).

I. INTRODUCTION AND REVIEW OF LITERATURE

At the present time there is great interest in sending space probes to explore the atmosphere of Jupiter. This involves accurate calculation of the heat transfer. In general, the heat transfer rate to the space vehicle depends on the transport phenomena (conduction, convection, diffusion, and chemical reactions) and radiative processes. Usually radiative heating becomes the major process for vehicles entering planetary atmospheres at hypersonic velocities. The heating is so severe that ablating heat shields are required. The ablation layer absorbs the radiant flux incident upon it reducing the radiation to the vehicle surface. The absorption in the ablation layer depends upon the spectral distribution of incident radiation and the absorption coefficient of species present in the vapor layer. Hence, the evaluation of the radiation energy transfer to the vehicle surface requires a knowledge of the shock layer temperature profile, and composition as well as the absorption coefficient of the species present in the shock layer.

The heat transfer problem for Jovian planetary probes is expected to involve entry velocities between 115,000 and 190,000 feet per second, ambient densities between 10^{-4} and 10^{-10} grams per cm^3, and ambient temperatures of 100 to $100^{o}K$[1]. The atmosphere of Jupiter consists mainly of atomic helium and molecular hydrogen. The most recent data

suggest that the composition in about 89% H_2, and 11% He[2]. The present study considers re-entry into a pure hydrogen atmosphere with a carbon ablation layer.

The calculation of equilibrium radiation from hydrogen plasmas has received considerable attention in recent years. Aroeste and Benton[3] described a method to estimate the total emissivity of hydrogen plasmas for temperature and pressure ranges in which hydrogen atoms are the major constituents. They calculated line transport in an approximate fashion and neglected the contribution due to the higher electronic levels. Olfe[4] considered hydrogen plasmas between 300°K and 10,000°K. He was mainly interested in molecular band radiation. Biberman et al[5] considered radiation from atomic hydrogen plasmas. They showed that line radiation (bound-bound) contributes most of the energy over a broad range of temperatures, pressures and layer thicknesses. Lasher, Wilson and Grief[6] calculated the energy radiated from an isothermal hydrogen plasma considering both line and continuum processes. They considered temperatures from 10,000°K to 40,000°K and pressures from 0.1 to 10 atmospheres. The principal line broadening mechanism was assumed to be stark broadening. They used detailed line profiles for the lower members of the Lyman and the Balmer series, while the higher members were assumed to have dispersion profiles. Their results agreed with those of Biberman, in that line radiation was very important.

Nelson and Goulard[1] investigated the radiation from equilibrium mixtures of helium and hydrogen in the range of pressures and temperatures relevant for a Jovian atmospheric penetration. They considered the pure hydrogen atmosphere as well as several other atmospheric compositions. Free-bound and free-free continuum were calculated using the methods reviewed by Griem[7]. They showed that the line radiation is usually more important than continuum radiation at low ambient densities. As the ambient density increases, the continuum radiation becomes the most important component of the emitted radiation, not only because of line saturation, but also because the plasma microfields reduce the ionization potential and thus eliminate many of the upper levels from which line transitions can take place.

Several papers studying the effect of ablation product gases injected into shock layer have been published in recent years. Howe and Sheaffer[8] investigated the effect of mass addition at hypersonic velocities in air. The gray gas approximation was employed, and the absorption properties of the ablation gases were assumed to be a multiple of those of air. Largely because of these approximations they found that mass addition exhanced, rather than reduced, the radiative flux to the surface. Hoshizaki and Lasher[9] studied the convective and radiactive heat transfer to an ablating body. They showed that absorption by ablation

products reduced the radiative flux by almost a factor of two. They considered re-entry into Earth's atmosphere with nylon and carbon phenolic as the ablators. Their results considered species composed of four elements: oxygen, nitrogen, carbon and hydrogen. They considered the molecular bands of C_2, CN, CO, and O_2, but neglected the atomic line transport. They reported that some preliminary calculations considering line transport did not alter the basic features of radiation coupled flow field, however; the radiative flux to the surface was increased. Furthermore, they found that the carbon atom was the most effective of the ablation species in reducing the radiation flux. The molecular species played a minor role but not a completely negligible one. Chin[10] investigated the effect of mass injection including line transitions for space vehicles re-entering the Earth's atmosphere. He considered essentially the same species as Hoshizaki and Lasher[9]. He included line transitions for nitrogen atoms but not those of the atoms present in the ablation gases. His results show that the ablation layer is very effective in reducing the wall heat flux, because the ablation layer effectively blocked all radiation fluxes with frequency greater than about 11 ev, because of the photo absorption of C ground and excited states, and H Lyman. Recently Wilson[11] reported a study of fully coupled viscous radiating shock layers including mass injection. He

considered a mixture of hydrogen, carbon, nitrogen and oxygen atoms as the ablation products and allowed for both line and continuum processes. His model was similar to that of Hoshizaki and Lasher[9] and Chin[10], except that he added many more lines including those of carbon, nitrogen and oxygen. However, he did not consider any molecular bands. He showed that including the line transport, particularly the carbon lines, resulted in a reduction of radiative flux which was only about one-half of the reduction calculated considering only continuum radiation. This reduction was due to reradiation by ablation product gases.

The present study investigates the effect of ablation layers on radiation from hydrogen plasmas using a very simple fluid dynamic model for the stagnation shock layer. The radiation model is taken to be as exact as possible. It allows for atomic lines and molecular bands as well as continuum processes. The next chapter introduces the physical model.

II. PHYSICAL MODEL

To simplify the fluid dynamics of the problem and yet keep the radiation calculations as exact as possible a two layer model was assumed to represent the stagnation shock layer. One layer contains only the species from the atmosphere, while the other contains only ablation species. This model is in agreement with the results of Hoshizaki and Lasher[9] which show that the ablation species exist in a thin layer close to the body, while the atmospheric species exist mainly in the region between the shock and ablation layer. In the current model which represents re-entry into Jupiter, one layer contains only hydrogen species and the other only carbon species (see Figure 1). The possible hydrogen species are: hydrogen atoms (H), the negative hydrogen ion (H^-), the molecular hydrogen ion (H_2^+), molecular hydrogen (H_2), electrons (e) and protons (P). The possible carbon species are: neutral carbon (C), singly ionized carbon (C^+), molecular carbon (C_2) and electrons (e). Each layer is assumed to have constant thermodynamic properties. The thermodynamic conditions in the hydrogen portion of the shock layer are determined as a function of the entry velocity of the vehicle and ambient density of the atmosphere by solving the Rankine-Hugoniot equations (see Appendix A). These give the temperature, pressure and density, which in turn, give the number density

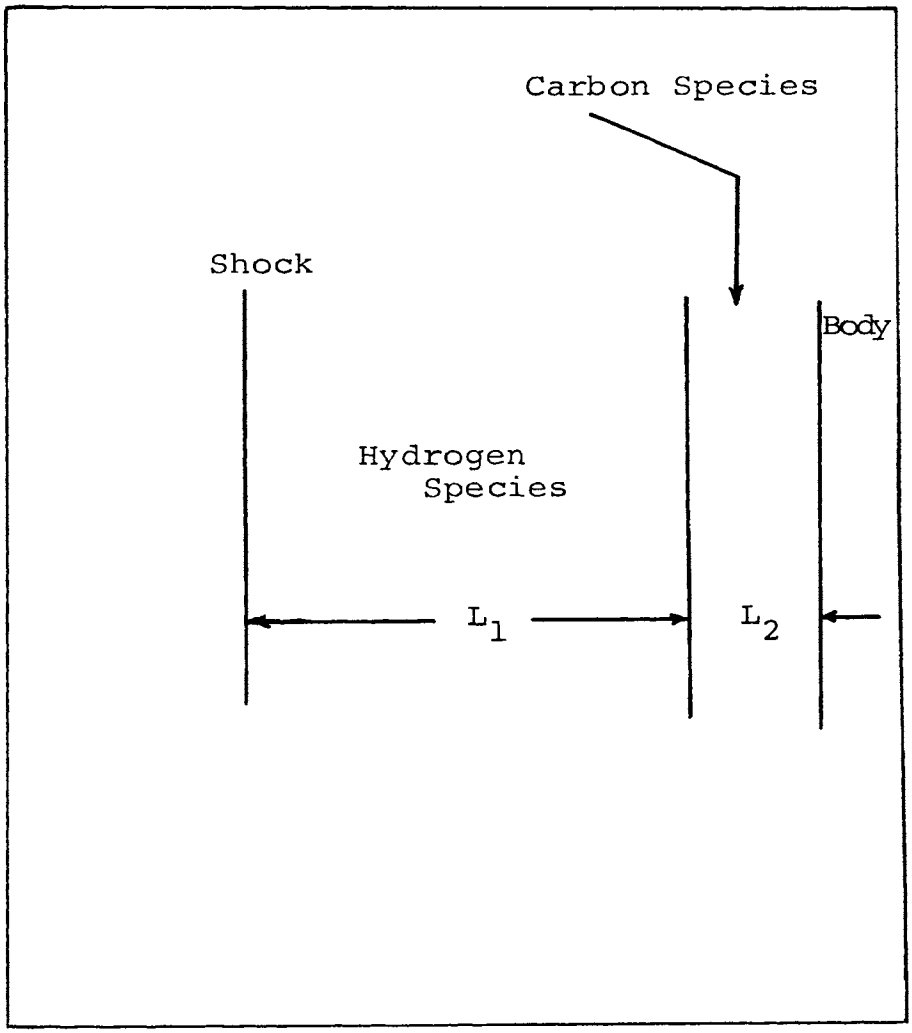

FIGURE 1. GEOMETRY OF SHOCK LAYER

of the species in the hydrogen layer.

The carbon layer temperature is taken as a parameter in the problem, and the carbon pressure is matched to that of the hydrogen layer, thus fixing the density. Thus, the model represents the shock layer by two layers, each at a different temperature and density, but both having the same pressure.

In the current study the shock layer thickness is taken to vary between 0.1 and 10 cm. The ablation layer thickness of up to 15% of the shock layer thickness are considered. This percentage thickness agrees with the results of Hoshizaki and Lasher[9]. The present study extends the work of Nelson and Goulard's[1] to include:

1) Hydrogen species H^-, H_2^+ and H_2 which they did not consider in their work.

2) Addition to an ablation layer which contains carbon type species. This layer is assumed to be at a temperature more closely representing the body surface temperature. Thus, the complete shock layer is no longer isothermal and homogeneous. It contains two layers which are at two different temperatures.

A. Equation of Transfer

To calculate the radiative flux, one must solve the radiative transfer equation. It may be written as[12]

$$\frac{dI_\nu}{dx} = k'_\nu \ (B_\nu - I_\nu) \qquad (2\text{-}1)$$

where I_ν is the radiant energy in the direction x per unit frequency, per unit time, per unit normal area; k'_ν is the effective absorption coefficient of the gas, i.e., k'_ν differs from the true coefficient k_ν by a factor allowing for induced emmission, $k'_\nu = k_\nu \ [1 - \exp(-h\nu/kT)]$; B_ν represents Planck's function

$$B_\nu(T) = \frac{2h\nu^3}{c^2(\exp(h\nu/kT)-1)} \ . \qquad (2\text{-}2)$$

The absorption coefficient represents both line (including the molecular bands) and continuum components

$$k'_\nu = k^l_\nu + k^c_\nu \qquad (2\text{-}3)$$

Equation (2-1) can be solved to give

$$I_\nu = B_\nu(T_1) \ [1 - \exp(- k'_\nu \ x)] \qquad (2\text{-}4)$$

for the case of an isothermal medium with no external radiation ($I_\nu(0) = 0$). For the current shock layer model Equation (2-4) gives the intensity of radiation emitted in the hydrogen layer at the interface of the hydrogen and carbon layer, if x is replaced by L_1. Attenuation by carbon layer must be considered to calculate the intensity at the wall; consequently, radiation transfer equation must be solved again for the carbon layer to get the

radiation intensity reaching the surface. The resulting expression is

$$I_{\nu w} = I_{\nu h} \exp(-k_\nu'^{(2)} L_2) + B_\nu(T_2)\,[1 - \exp(-k_\nu'^{(2)} L_2)] \tag{2-5}$$

where the boundary condition is $I_\nu(L_2 = 0) = I_{\nu h}$, as given by Equation (2-4). The superscript 1 is used to represent the hydrogen layer, and 2 is used to represent the carbon layer.

The one-sided heat flux at the body surface is given by

$$F_{\nu w} = 2\pi \int_0^1 I_{\nu w}\, \mu\, d\mu \tag{2-6}$$

where $\mu = \cos^{-1}\theta$. From Equations (2-5) and (2-6) the raditive flux to the body surface becomes

$$F_{\nu w} = 2\pi\,[B_\nu(T_1)\{E_3(k_\nu'^{(2)} L_2) - E_3(k_\nu'^{(1)} L_1 + k_\nu'^{(2)} L_2)\} + B_\nu(T_2)(1/2 - E_3(k_\nu'^{(2)} L_2))] \tag{2-7}$$

where E_3 is the exponential integral of order three[12].

Total intensity and total flux at the body are obtained by integrating Equations (2-5) and (2-7) over frequency from 0 to ∞.

$$I_w = \int_0^\infty I_{\nu w}\, d\nu \tag{2-8}$$

$$F_w = \int_0^\infty F_{\nu w} \, d\nu \qquad (2\text{-}9)$$

In order to evaluate the radiative flux and intensity reaching the body, one must know the absorption coefficient for each of the species present in the shock layer as well as the number densities of each species. Chapter III contains the details of the composition calculations, while Chapter IV lists the absorption coefficients for each of the possible species in the shock layer. The radiative heat transfer results obtained from this model are discussed in Chapter V.

III. COMPOSITION

This chapter contains the basic equations which are necessary to calculate the shock layer composition. Section A considers the ablation layer while section B considers the hydrogen layer.

A. Ablation Layer

The ablation layer is allowed to contain only the species C_2, C, C^+ and e. At the temperatures of interest, the following reactions must be considered.

$$C_2 \rightleftharpoons 2C \qquad (3\text{-}1)$$

$$C \rightleftharpoons C^+ + e^- \qquad (3\text{-}2)$$

Consider a system composed of M carbon nuclei at a given volume V and temperature T. Let α be the fraction of carbon nuclei that are present as carbon molecules, so that $\alpha M/2$ is the number density of carbon molecules. Let β be the fraction of the carbon nuclei that are free, that is exist as C^+, the βM is the number density of C^+. For each C^+ formed an electron is also freed thus, then the number density of electrons is also equal to βM. The remaining nuclei are present as neutral carbon atoms. Therefore, the number density of carbon atoms is $(1 - \beta - \alpha)M$. The total numbers of particles in the system is given by

$$N = (1 + \beta - \alpha/2)M, \tag{3-3}$$

so that the gas pressure is

$$P = (1 + \beta - \alpha/2)\ MkT, \tag{3-4}$$

where k is the Boltzmann constant.

Applying the law of mass action to reaction (3.1) one can write[13]

$$\frac{AN_{C_2}}{N_C^2} = RT \exp \frac{-\Delta F_T^0}{RT} = RTk_p \tag{3-5}$$

where R is the universal gas constant, ΔF_T^o is the change in free energy at temperature T for the reaction, k_p is the equilibrium constant for the reaction and A is the Avagadro's number.

For reaction (3.2) using Saha equation one can write[13]

$$\frac{AN_C}{N_{C^+}^2} = A\left(\frac{h^2 m_C}{2\pi kT m_{e^+} m_{c^+}}\right)^{3/2} \frac{Q_C}{Q_e Q_{c^+}} \exp\ (I/kT) = RTk_p^+ \tag{3-6}$$

where k_p^+ is the equilibrium constant for the reaction, h is Planck's constant, I is the ionization potential of carbon, and Q's are the electronic partition functions of the species represented by the subscripts. The partition functions are taken from Gilmore[13], and are tabulated in Appendix B.

Curve fits of the free energy function were taken from references (14 and 15). The expressions used are presented in Appendix B.

The equations were solved as follows. The temperature and pressure in the ablation layer are both assumed to be known. Thus, the right hand side of Equations 3-5 and 3-6 are known.

Substituting the values of number densities in terms of α and β, one can write

$$\frac{(1 - \beta - \alpha) M}{\beta^2 M^2} = \frac{R}{A} T k_p^+ \qquad (3-7)$$

and

$$\frac{\alpha M}{2(1 - \beta - \alpha)^2 M^2} = \frac{R}{A} T k_p \qquad (3-8)$$

where

$$M = \frac{P}{(1 + \beta - \frac{\alpha}{2}) kT} \qquad (3-9)$$

Simplifying (3-7) and (3-8) using (3-9) gives

$$2\beta^2 (1 + Pk_p^+) + \alpha\beta + 3\alpha - \alpha^2 - 2 = 0 \qquad (3-10)$$

and

$$\beta^2 (2Pk_p) + \alpha\beta(4k_p p - 1) - \beta(4Pk_p) - \alpha(4Pk_p + 1) + \alpha^2 (2Pk_p + 1/2) + 2Pk_p = 0, \qquad (3-11)$$

where α and β are always between 0 and 1.

Equation (3-10) and (3-11) were solved by an interation process. The process begins by assuming $\beta = 0$ and solving for α using Equation (3-11), which represented the dissociation of molecular carbon.

$$\alpha^{(0)} = (4Pk_p + 1) \pm \sqrt{(4Pk_p + 1)^2 - 8Pk_p\,(2Pk_p + 1/2)} \tag{3-12}$$

then using the value of $\alpha^{(0)}$ (the root which lies between 0 and 1) in Equation (3-10) $\beta^{(1)}$ is given as

$$\beta^{(1)} = -\alpha^{(0)} \pm \sqrt{\alpha^{(0)2} - 4(1 + Pk_p^+)(3\alpha^{(0)} - \alpha^{(0)2} - 2)} \tag{3-13}$$

Equation (3-11) is then solved with $\beta = \beta^{(1)}$ giving $\alpha^{(1)}$ as

$$\alpha^{(1)} = \frac{(4Pk_p + 1) - \beta(4Pk_p - 1) \pm \sqrt{[(4Pk_p + 1 -}}{\beta(4Pk_p - 1)]^2 - 4(2Pk_p + 1/2)(2Pk_p + 2\beta^2 Pk_p - 4\beta Pk_p)} \tag{3-14}$$

This process is continued until two successive values of α and two successive values of β agree to 5 places. Convergence usually occurred in less than 20 iterations. Once α and β are known all the number densities can be obtained.

Figures (2-4) give the equilibrium composition of a carbon plasma as a function of temperature for pressures of

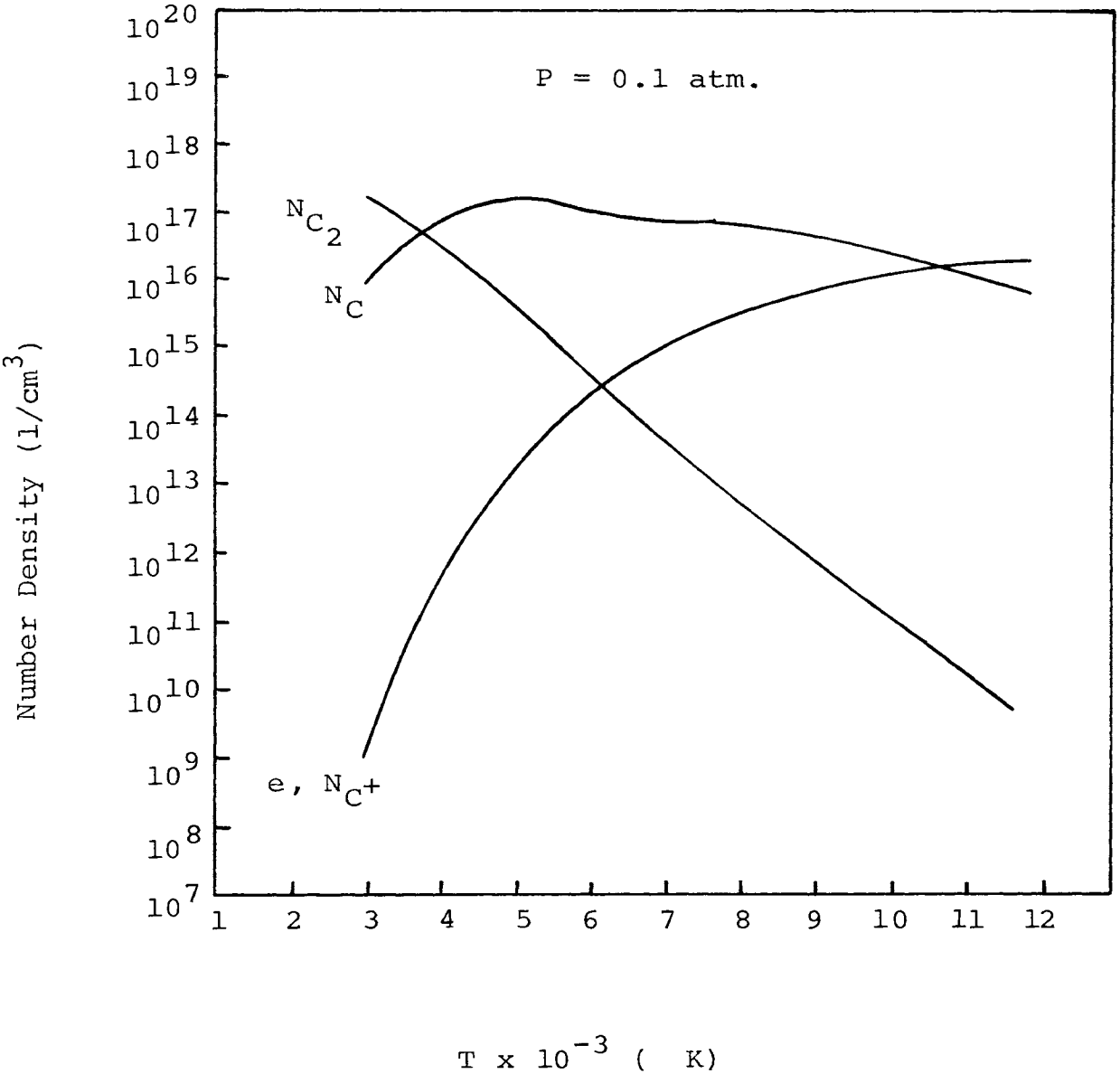

FIGURE 2. EQUILIBRIUM COMPOSITION OF CARBON

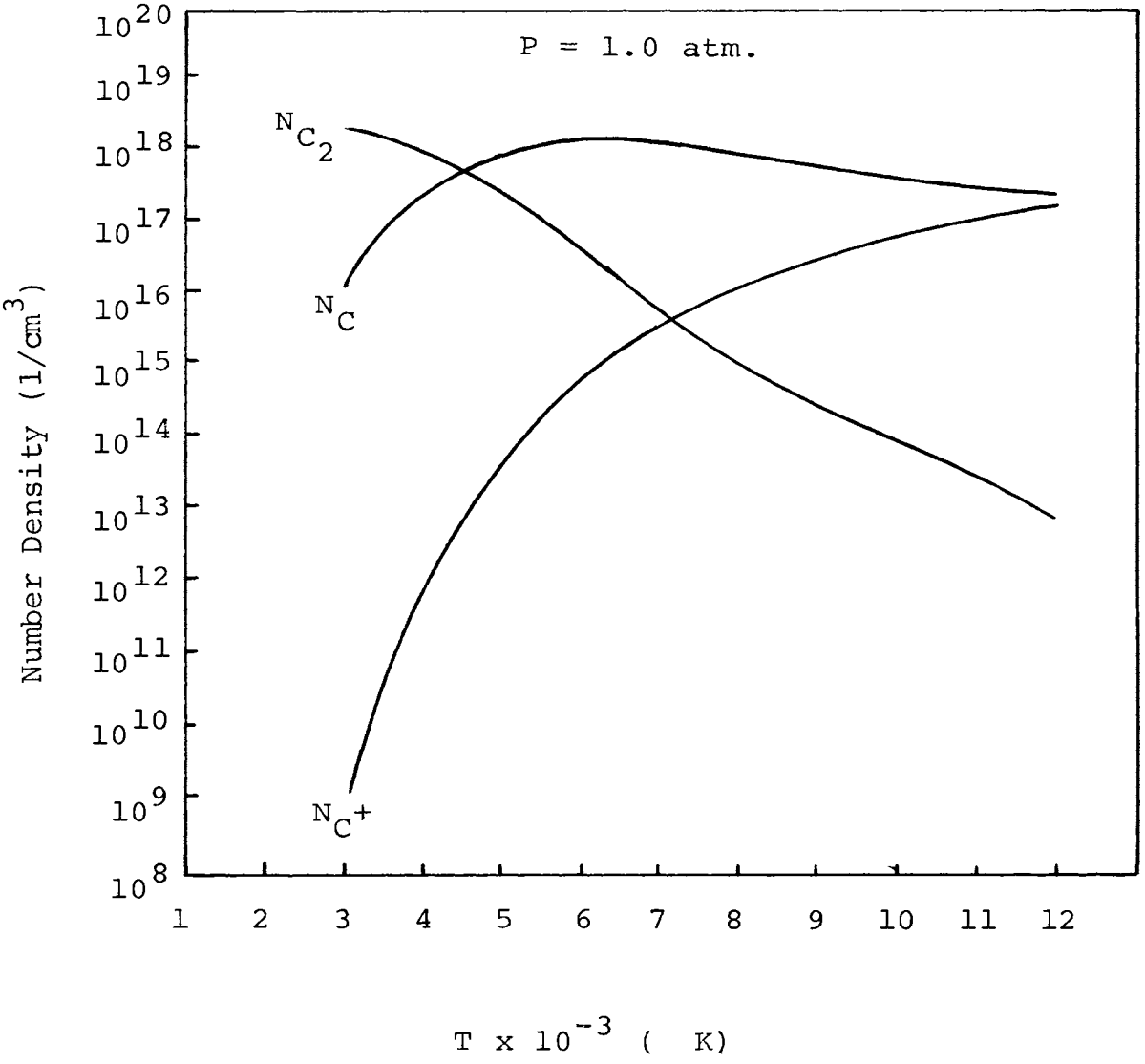

FIGURE 3. EQUILIBRIUM COMPOSITION OF CARBON

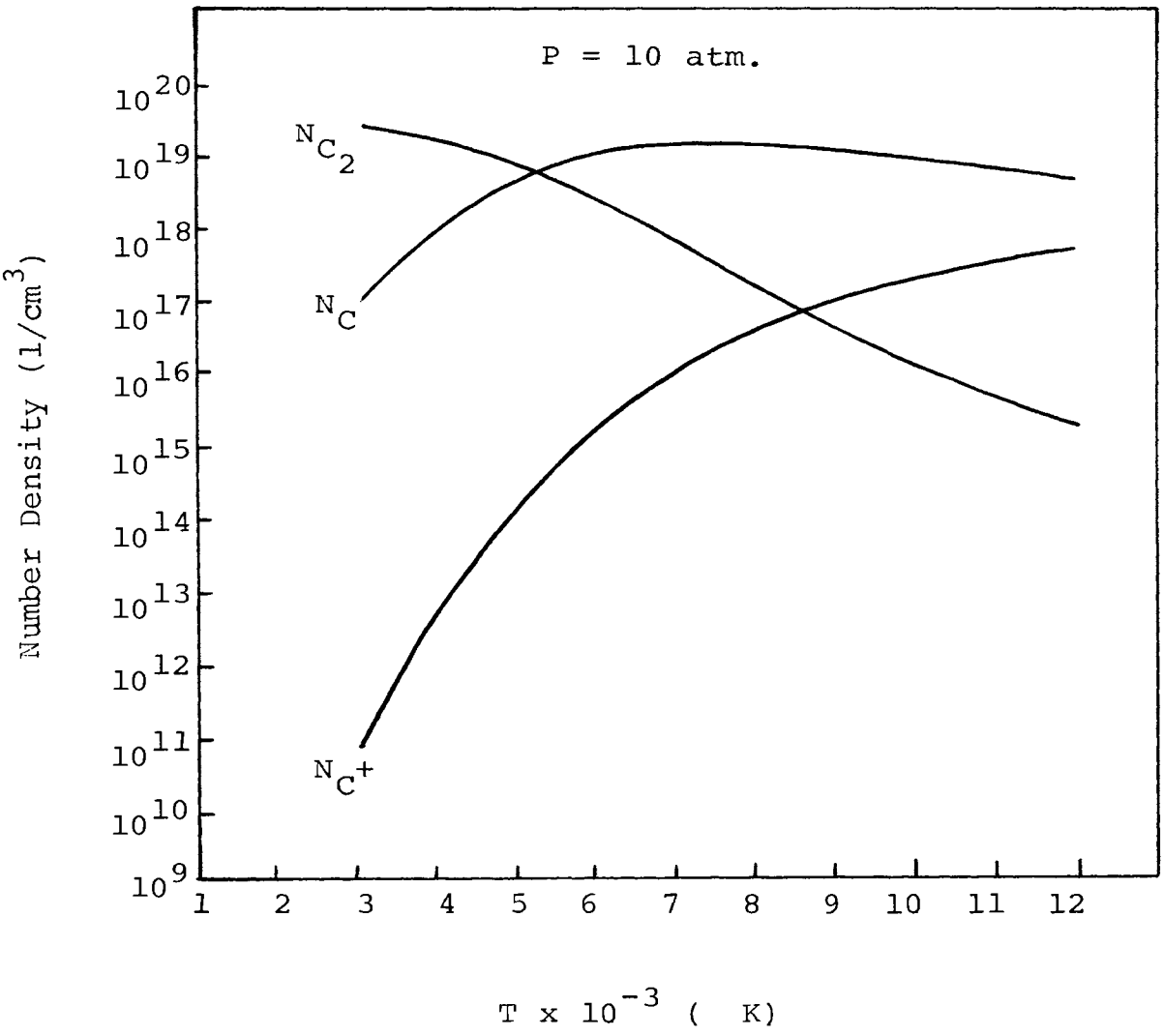

FIGURE 4. EQUILIBRIUM COMPOSITION OF CARBON

.1, 1.0 and 10 atmospheres. Notice that molecular carbon is essentially the only species present at temperatures below 3000°K, while at temperatures of 7000°K which is the highest ablation layer temperature considered in this study, the carbom atom is the most important species. At a constant value of temperature more molecular carbon is present at high pressures than at low pressures. Also, the number of singly ionized carbon particles increases as the temperature increases and as the pressure decreases.

B. Hydrogen Layer

To calculate the equilibrium composition of hydrogen plasma at high temperatures, the following reactions must be considered.

$$H_2 \rightleftharpoons H + H \tag{3-15a}$$

$$H \rightleftharpoons P + e \tag{3-15b}$$

$$H + e \rightleftharpoons H^- \tag{3-15c}$$

$$H_2 \rightleftharpoons H_2^+ + e \tag{3-15d}$$

The total number of hydrogen molecules is

$$N'_{H_2} = \rho/m_{H_2} \tag{3-16}$$

where the gas density ρ is assumed to be known. The hydrogen layer temperature is also known from the solutions of Rankine-Hugoniot equations.

Let ξ be the fraction of the molecular hydrogen that has dissociated (Equation 3-15a); therefore, the number density of molecular hydrogen is $(1 - \xi)N'_{H_2}$, while $N_H = 2\ \xi N'_{H_2}$, because two hydrogen atoms are formed in each dissociation process.

Let α be the fraction of N_H that exists as protons, then $N_P = 2\alpha\xi N'_{H_2}$. For each proton that is formed an electron also becomes free; therefore, $N_e = N_P$. The number density of remaining atomic hydrogen is $N_H = 2\xi(1 - \alpha)\ N'_{H_2}$.

The negative hydrogen ion is formed by the reaction given in Equation (3.15c). Let δ be the fraction of atomic hydrogen that exists as the negative hydrogen ion, then $N_{H^-} = \delta(1 - \alpha)\ 2\xi N'_{H_2}$. The remaining number density of atomic hydrogen is $N_H = (1 - \delta)(1 - \alpha)\ 2\xi N'_{H_2}$ and that of the electrons is $N_e = 2\xi[\alpha - \delta(1 - \alpha)]N'_{H_2}$, because an electron is used for each H^- that is formed.

In addition the molecular ion H_2^+ is formed by the process of Equation (3.15d). Let η be the fraction of H_2 that exists as H_2^+. Then $N_{H_2^+} = \eta\ (1 - \xi)\ N'_{H_2}$ and $N_{H_2} = (1 - \eta)\ (1 - \xi)\ N'_{H_2}$. For each H_2^+ ion that is formed an electron becomes free; therefore, the electron number density becomes $N_e = [(\alpha - \delta)(1 - \alpha))2\xi + \eta(1 - \xi)]N'_{H_2}$.

In summary, the final number densities are related to the initial number densities as follows:

$$N_{H_2} = (1 - \eta)(1 - \xi)\ N'_{H_2} \qquad (3\text{-}17a)$$

$$N_H = 2\xi(1 - \alpha)(1 - \delta)N'_{H_2} \tag{3-17b}$$

$$N_P = 2\alpha\xi\, N'_{H_2} \tag{3-17c}$$

$$N_{H^-} = 2\xi(1 - \alpha)\delta N'_{H_2} \tag{3-17d}$$

$$N_{H_2^+} = \eta(1 - \xi)N'_{H_2} \tag{3-17e}$$

$$N_e = [2\xi(\alpha - \delta(1 - \alpha) + \eta(1 - \xi)]N'_{H_2} \tag{3-17f}$$

The condition of macroscopic neutrality

$$N_e + N_{H^-} = N_P + N_{H_2^+} \tag{3-18}$$

as well as the conservation of nuclei are satisfied identically by the relations of Equation (3-17).

The equilibrium relationships between the atoms and ions as defined in Equation (3-15) are given in terms of the complete partition functions as

$$kT\,\frac{N_P N_e}{N_H} = \frac{\alpha P_e}{(1 - \delta)(1 - \alpha)} = \frac{Z_P Z_e}{Z_H}\,kT = \beta_3, \tag{3-19}$$

$$kT\,\frac{N_H N_H}{N_{H_2}} = \frac{[2\xi(1 - \delta)(1 - \alpha)]^2}{(1 - \eta)(1 - \xi)} = \frac{Z_H Z_H}{Z_{H_2} N'_{H_2}} = \beta_4, \tag{3-20}$$

$$kT\,\frac{N_H N_e}{N_{H^-}} = \frac{(1 - \delta)P_e}{\delta} = \frac{Z_H Z_e}{Z_{H^-}}\,kT = \beta_5, \tag{3-21}$$

and

$$kT\,\frac{N_{H_2^+} N_e}{N_{H_2}} = \frac{\eta P_e}{1-\eta} = \frac{Z_{H_2^+} Z_e}{Z_{H_2}}\,kT = \beta_6, \tag{3-22}$$

where the electron pressure P_e is defined as

$$P_e = [2\xi(\alpha - \delta(1 - \alpha)) + \eta(1 - \xi)]N'_{H_2}\ kT. \quad (3\text{-}23)$$

The partition functions are defined in Appendix B.

The set of Equations (3-19) through (3-23) represents five unknowns; α, ξ, δ, η and P_e, which can be found as functions of temperature and density.

An iterative method is used to solve the set of Equations (3-19) through (3-22). The solution begins by assuming $\delta = \eta = 0$. Thus, Equations (3-19) through (3-23) become

$$\alpha P_e = \beta_3\ (1 - \alpha) \quad (3\text{-}24)$$

$$4\xi^2(1 - \alpha)^2 = \beta_4(1 - \xi) \quad (3\text{-}25)$$

$$P_e = 2\xi\alpha N'_{H_2}\ kT \quad (3\text{-}26)$$

Eliminating P_e and ξ one arrives at an equation in terms of α

$$(1 - \alpha)^4\left[\frac{\beta_3}{kT\ N'_{H_2}}\right]^2 + \frac{(1 - \alpha)\alpha^2}{2}\ \frac{\beta_3\beta_4}{kT} - \alpha^4\beta_4 = 0 \quad (3\text{-}27)$$

which can be solved to give the initial value of α, $(\alpha^{(0)})$. Combining Equations (3-26) and (3-24) and using $\alpha^{(0)}$, the initial value of ξ becomes

$$\xi^{(0)} = \frac{1 - \alpha^{(0)}}{2(\alpha^{(0)})^2}\ \frac{\beta_3}{kTN'_{H_2}} \quad (3\text{-}28)$$

and the other initial values become

$$P_e^{(0)} = 2\xi^{(0)}\ \alpha^{(0)}\ N'_{H_2}\ kT \tag{3-29}$$

$$\delta^{(0)} = \frac{P_e^{(0)}}{P_e^{(0)} + \beta_5} \tag{3-30}$$

$$\eta^{(0)} = \frac{\beta_6}{\beta_6 + P_e^{(0)}} \tag{3-31}$$

Once the initial values are known the ith value of the variable is arrived at in the following manner.

$$P_e^{(i)} = \{2\xi^{(J)}[\alpha^{(J)}(1 + \delta^{(J)}) - \delta^{(J)}] + \eta^{(J)}(1 - \xi^{(J)})\}$$

$$N'_{H_2}\ kT \tag{3-32}$$

$$\eta^{(i)} = \frac{\beta_6}{\beta_6 + P_e^{(i)}} \tag{3-33}$$

$$\delta^{(i)} = \frac{P_e^{(i)}}{P_e^{(i)} + \beta_5} \tag{3-34}$$

$$\alpha^{(i)} = \frac{\beta_3(1 - \delta^{(i)})}{P_e^{(i)} + \beta_3(1 - \delta^{(i)})} \tag{3-35}$$

$$\xi^{(i)} = \frac{X^{(i)}}{2}\{[1 + \frac{4}{X^{(i)}}]^{1/2} - 1\} \tag{3-36}$$

where

$$X^{(i)} = \frac{\beta_4(1 - \eta^{(i)})}{4(1 - \delta^{(i)})(1 - \alpha^{(i)})^2} \tag{3-37}$$

and

$$J = i - 1$$

The iteration is continued until successive values of P_e are the same to a specified number of places.

Figures (5) and (6) show the equilibrium composition of hydrogen plasmas as a function of temperature for $\rho = 10^{-6}$ and $\rho = 10^{-7}$ grams/cm^3. At a given density as temperature increases, the number density of atomic hydrogen rapidly decreases initially and then becomes almost constant at higher temperatures. The number density of electrons and protons initially increases and then becomes almost constant at higher temperatures when the plasma is fully ionized. Note that molecular hydrogen is unimportant at temperatures above 10,000^{o}K.

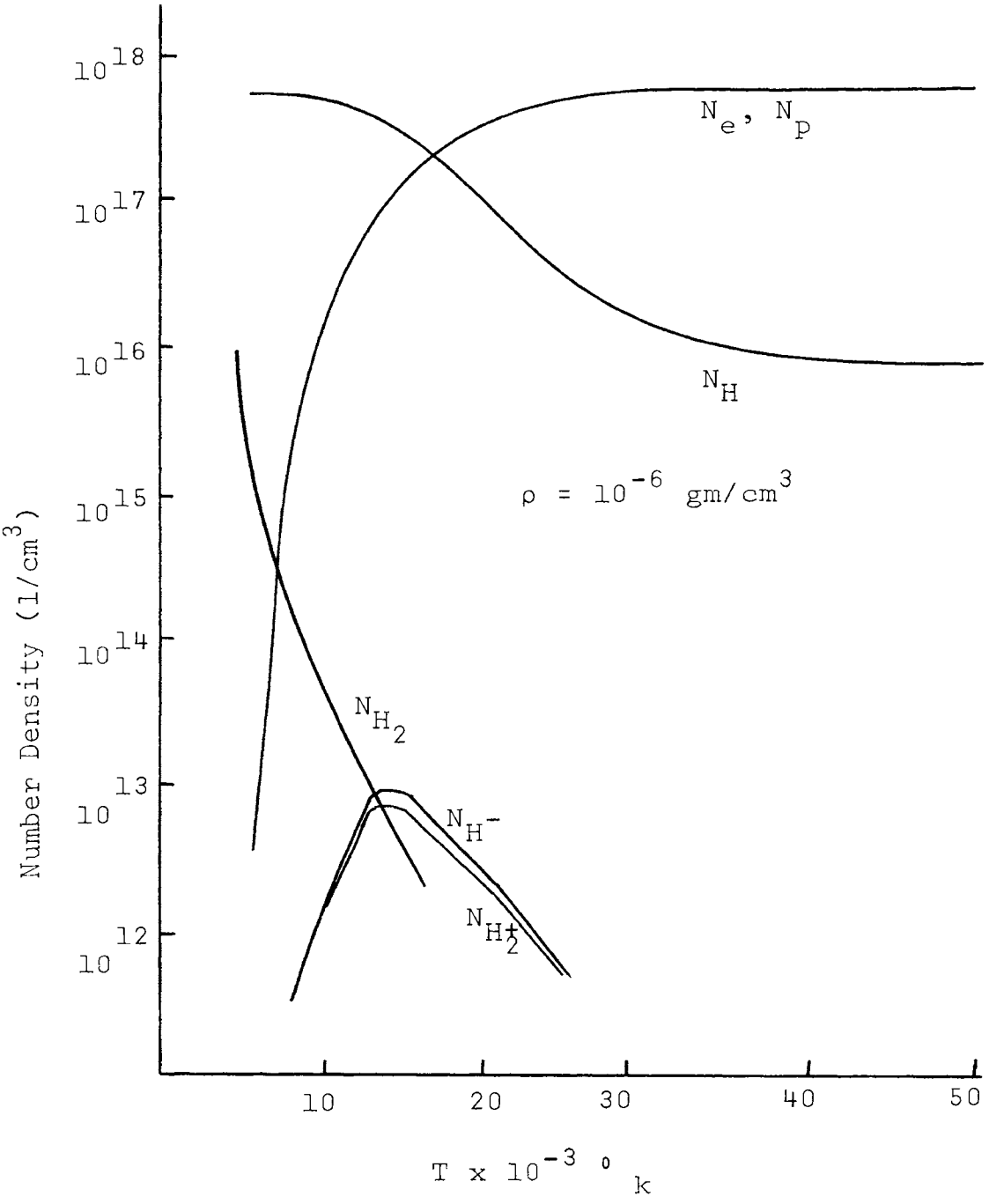

FIGURE 5. EQUILIBRIUM COMPOSITION OF HYDROGEN

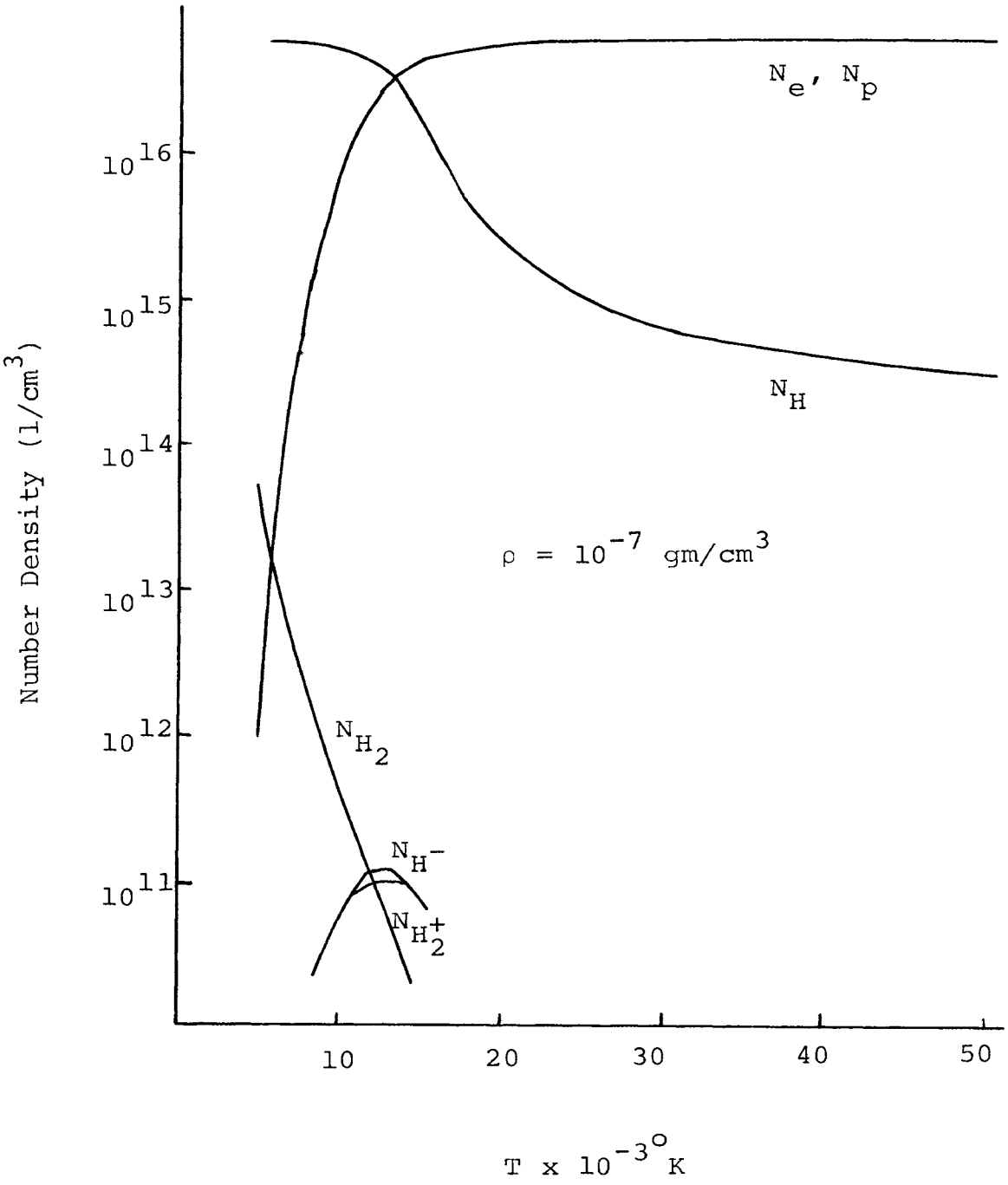

FIGURE 6. EQUILIBRIUM COMPOSITION OF HYDROGEN

IV. ABSORPTION COEFFICIENTS

The radiation absorption coefficient reflects the type of transition that is taking place. For atomic gases one only has to consider electronic transitions and ionization, but for a molecular gas one must consider rotational and bivrational transitions and dissociation. The radiation absorption coefficient relates these physical processes to the energy of the radiation field. Free-free and bound-free transitions result in continuous absorption and emission spectra. Bound-bound transitions form line spectra in atoms, while in molecules it results in the formation of band spectra. Both the line and continuum processes as well as the molecular bands of carbon are considered in this study.

A. Line Absorption Coefficient for Atomic Carbon and Singly Ionized Carbon

The absorption cross-section of a line may be written for the transition $\ell \rightarrow u$ as[16]

$$\sigma_{\ell u}(\nu) = \frac{\pi e^2}{mc} f_{\ell u} b_{\ell u}(\nu) \qquad (4\text{-}1)$$

where $b_{\ell u}(\nu)$ represents the shape of the line, normalized according to

$$\int_0^\infty b_{\ell u}(\nu)\, d\nu = 1 \qquad (4\text{-}2)$$

For the plasma conditions of interest, the most important line broadening mechanism is electronic Stark broadening[7]. In the electron impact approximation the lines acquire a Lorentz shape[17,18]

$$b_{\ell u}(\nu) = \frac{(\gamma_{\ell u})/\pi}{[\nu - \nu_{\ell u}]^2 + (\gamma_{\ell u})^2} \qquad (4\text{-}3)$$

where ν_u is the frequency corresponding to the unperturbed transition from state ℓ to u, and $\gamma_{\ell u}$ is the half(half) width of the line.

To obtain the bound-bound absorption coefficient k_ν, the cross-section is multiplied by the occupation number N_ℓ of state ℓ (the number density of a given species in state ℓ). For a monoatomic gas in local thermodynamic equilibrium the population of the ℓth electronic state is given by the Boltsman formula

$$N_\ell = (g_\ell/Q)N \exp(-E_\ell/kT) \qquad (4\text{-}4)$$

where Q represents the electronic partition function. The energy levels, partition functions, and statistical weights for carbon atoms and ions are taken from Gilmore[13] and are listed in Appendix B. The normalized half-widths ($\bar{\gamma}_{\ell u} = \gamma_{\ell u}/N_e$ and $\nu_{\ell u}$ are tabulated by Wilson and Nicolet[18]. The f numbers are taken from Wiese, Smith and Glennon[19].

The 19 carbon lines and 9 singly ionized carbon lines as well as the f-numbers and half-widths are listed in Table I.

B. Continuum Absorption Coefficient for Atomic Carbon and Singly Ionized Carbon

The continuum transport of carbon is calculated using a multi-band model. Each band represents a given spectral region. In each band the absorption coefficient is given by

$$k_\nu^C = N_C \sigma_C + N_{C^+} \sigma_{C^+} \qquad (4\text{-}5)$$

The values of absorption cross-sections for neutral carbon and singly ionized carbon are taken from Wilson and Nicolet[18]. The equations for the absorption cross-sections for each spectral region are listed in Appendix C.

The absorption cross-sections of atomic carbon and singly ionized carbon at $5000^{\circ}K$ are plotted as a function of frequency in Figures 7 and 8, respectively.

C. Molecular Absorption Coefficient for Carbon Bonds

The four molecular bands considered were the; 1) Swan; 2) Mulliken; 3) Freymark and 4) Fox-Herzberg. The absorption cross-sections for each band was fitted to the values given by Hoshizaki and Lasher[9]. The data given by Hoshizaki and Lasher[9] was at a specific temperature which gave the maximum values for the cross-section of interest. No attempt was made in the current study to allow the band cross-section

TABLE I Carbon Lines

	Neutral Carbon			Singly Ionized Carbon		
No.	λ (A[1])	f-number	$\overline{\gamma}_{\ell u}$ (ev)	λ (A)	f-number	$\overline{\gamma}_{\ell u}$ (ev)
1	911.33	.295	1.34E-22	636	.0105	1.63E-21
2	944.81	.27	1.21E-21	641.66	.165	2.02E-22
3	1017.6	1.05	1.34E-22	651.24	.488	2.02E-22
4	1140.0	.705	8.82E-20	688.08	.26	2.03E-22
5	1260	.029	2.32E-21	808.23	.123	3.04E-22
6	1277	.063	1.81E-21	858.08	.046	3.00E-22
7	1328	.038	3.09E-23	903.76	.52	3.54E-23
8	1463	.093	1.89E-21	1036.4	.059	1.93E-23
9	1481	.011	1.56E-21	1335	.27	1.47E-23
10	1560	.091	8.99E-23			
11	1657	.17	6.98E-22			
12	1929	.082	9.01E-22			
13	2478	.094	9.01E-22			
14	8336	.11	1.74E-21			
15	9061	.31	1.01E-21			
16	9601	.1	9.22E-22			
17	10658	.5	8.20E-22			
18	11330	.65	1.56E-21			
19	11638	.132	1.81E-21			

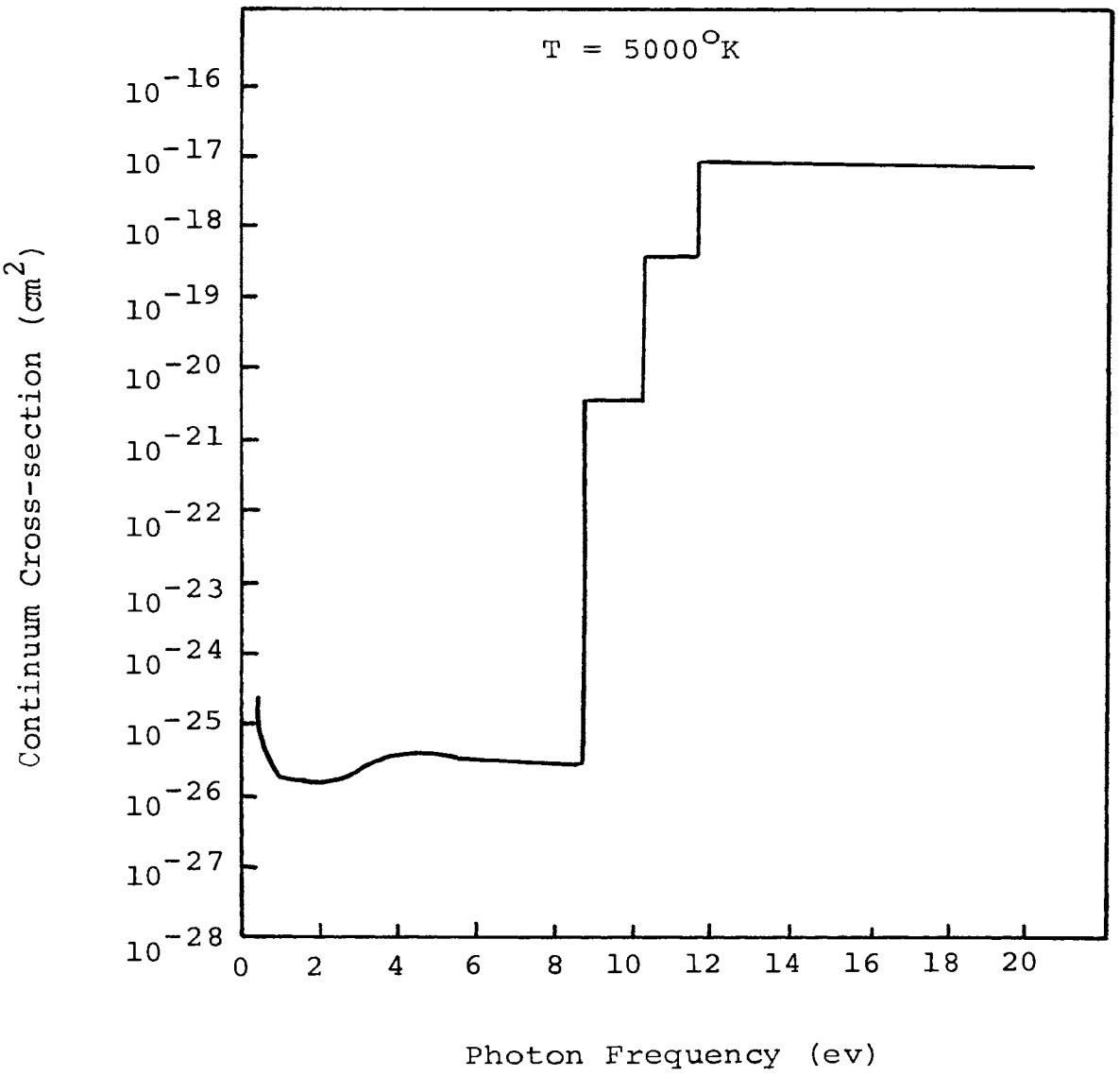

FIGURE 7. TOTAL EFFECTIVE CONTINUUM CROSS-SECTION FOR NEUTRAL CARBON ATOMS

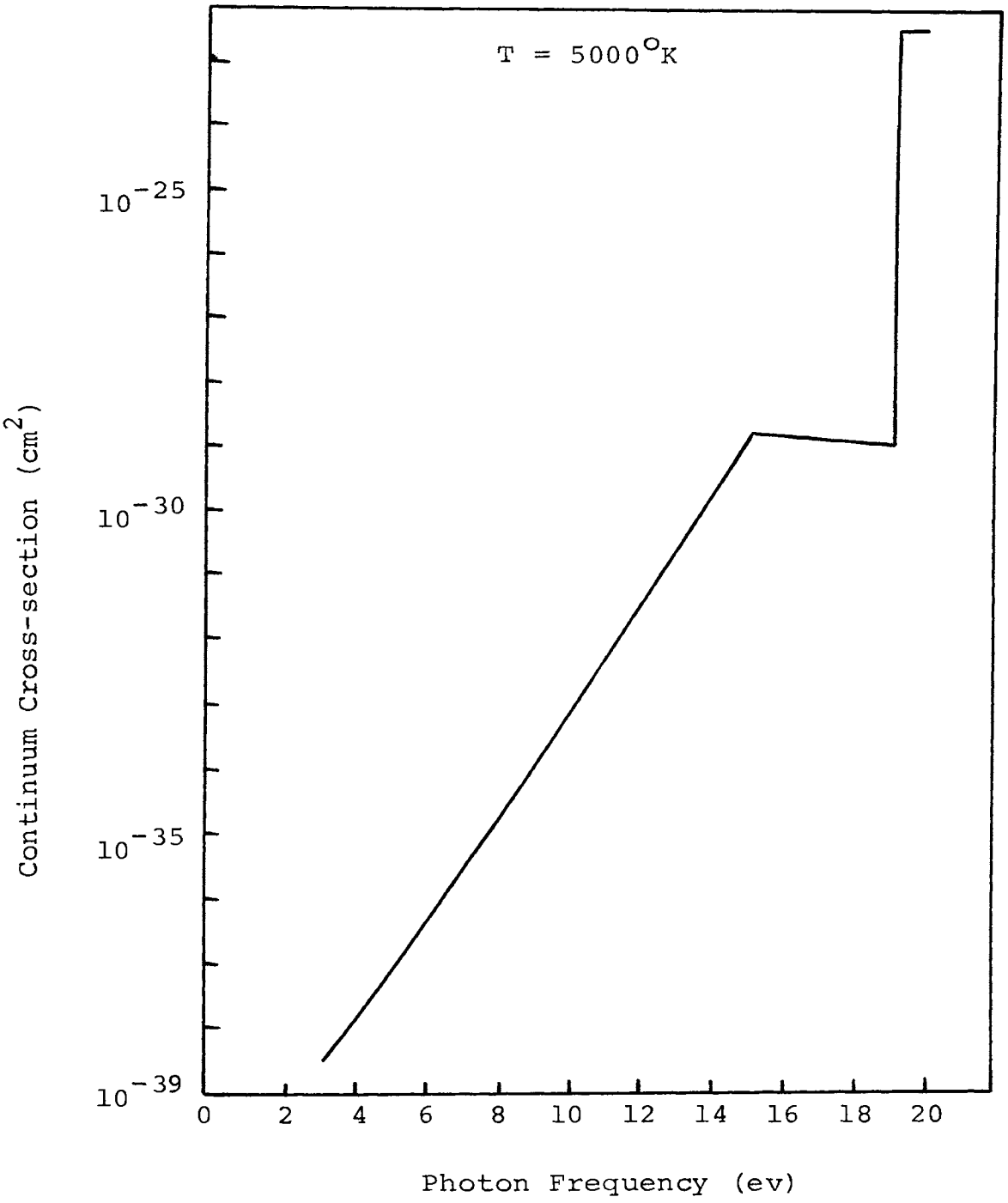

FIGURE 8. TOTAL EFFECTIVE CONTINUUM CROSS-SECTION FOR SINGLY IONIZED CARBON

to change with temperature. The band cross-sections are listed in Appendix C.

D. Line Absorption Coefficient for Atomic Hydrogen

The line absorption coefficient for atomic hydrogen is treated in the same manner as done by Nelson and Goulard[1]. The lines considered were Lyman, Balmer, Paschen, and Brackett. The line shapes for L_α, L_β, H_α, H_β, H_γ, and H_δ were taken from Griem[7]. The higher transitions involving electronic levels through the 12th were assumed to have a dispersion shape. Transitions involving the levels 13 and above are ignored because of their small energy. All the f numbers and Einstein coefficients used in their calculations were taken from the tables compiled by Wiese, Smith and Glennon[19].

E. Continuum Absorption Coefficient for Atomic Hydrogen

The continuum radiation consists of two parts, bound-free and free-free. The continuum absorption coefficient for atomic hydrogen is[7]

$$k_\nu = \frac{32}{3\sqrt{3}} \frac{\pi^2 e^6 R_H}{h^3} N_1 \frac{e^{-X_1}}{\nu^3} \{\sum_{\nu_{n<\nu}}^{X_5} \frac{e^{X_n}}{n^3} g_{bf} + \frac{e^{(X_6-1)}}{2X_1} + \frac{g_{ff}}{2X_1}\}, \tag{4-6}$$

where

$$X_n = \frac{c_h R_h}{n^2 kT}, \tag{4-7}$$

$$\nu_n = \frac{cR_H}{n^2} , \qquad (4\text{-}8)$$

and N_1 is the population of ground state of hydrogen. The summation includes only those levels for which ν is greater than ν_n and n is less than 6. The second term contains the effect of levels 6 and greater, while the third term represents the free-free transitions. The bound-free θ Gaunt factor is (20).

$$g_{bf} = 1 + .1728 \left(\frac{\nu}{2R_H}\right)^{1/3} \left(\frac{2cR_H}{n^2\nu} - 1\right) \qquad (4\text{-}9)$$

and the free-free Gaunt factor is[20].

$$g_{ff} = 1 + .1728 \left(\frac{\nu}{2R_H}\right)^{1/3} \left(1 + \frac{2kT}{h\nu}\right) \qquad (4\text{-}10)$$

The absorption coefficient for H_2^+ is taken from Bozess[21] and that for H^- is taken from Darwin and Felenbok[22]. Detailed discussions for these are presented in Appendix C.

The total absorption coefficient for hydrogen at a temperature of $17958^{o}K$ is plotted as a function of frequency in Figure 9.

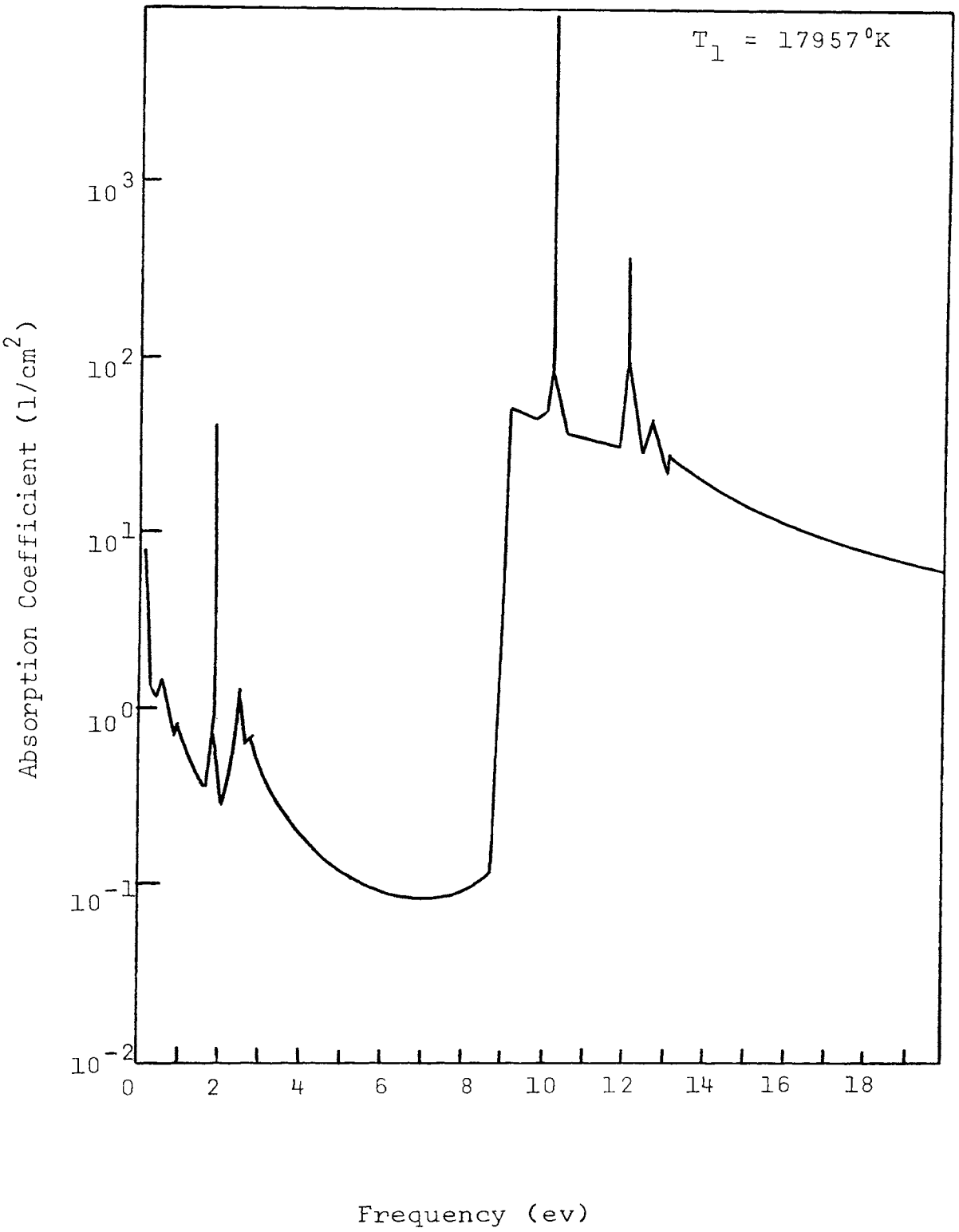

FIGURE 9. SPECTRAL ABSORPTION COEFFICIENT FOR HYDROGEN

V. RESULTS AND DISCUSSION

The shock layer radiation was calculated for an ambient density range of 10^{-6} to 10^{-9} grams/cm^3, at entry velocities of 115,000 and 190,000 feet per second. The ambient atmosphere was assumed to be pure hydrogen. The shock layer, as stated before, was assumed to be composed of two plane parallel layers; one containing hydrogen species and other carbon species. Each layer was assumed to be isothermal and in thermodynamic equilibrium at its respective temperature. The Rankine-Hugoniot Equations were solved to give the thermodynamic conditions in the hydrogen portion of the shock layer (see Equations (A-1) to (A-5)). The carbon layer temperature was taken as a parameter in the problem (values used were; 3000, 5000 and 7000°K) and its pressure was watched to that of the hydrogen layer.

To investigate the influence of different layer thickness, four ratios of the ablation layer thickness to the total shock layer thickness were considered; 1) 0.0, 2) .05, 3) .10 and 4) .15. For each of these ratios the total flux and total intensity as well as the fluxes and intensities for the combinations; 1) hydrogen and carbon lines (including carbon bands), 2) hydrogen and carbon continuum and 3) hydrogen lines and carbon continuum were calculated. The influence of shock layer thickness was also

investigated by allowing the total shock layer thickness to vary from .1 cm at a velocity of 190,000 ft. per second and density of 10^{-7} gm/cm^3.

The calculations were performed numerically on the IBM-360 Model 50 Digital Computer. Simpson's rule was used to perform the frequency integration as given by Equations (2-8) and (2-9). The high velocity, high density cases took about 10 minutes of computer time, while the low velocity, low density cases took up to 40 minutes. Detailed results of all the data are presented in tabular form in Appendix D.

A. Influence of the Carbon Layer in Reducing the Radiation to the Body

Figures 10 and 11 show the percentage change in the radiative flux to the surface as a function of the ratio of the ablation layer thickness to hydrogen layer thickness for several ambient densities. Figure 10 gives the results for a velocity of 190,000 feet per second and Figure 11 for 115,000 feet per second. The carbon layer temperature was taken to be 5000^{o}K for these cases.

At 190,000 feet per second the effectiveness of the ablation layer in reducing the flux to the surface increases as the density increases. The number density of the carbon species is directly proportional to the shock layer pressure, which is proportional to the ambient density. Thus, as the density increases, the optical thickness of carbon layer

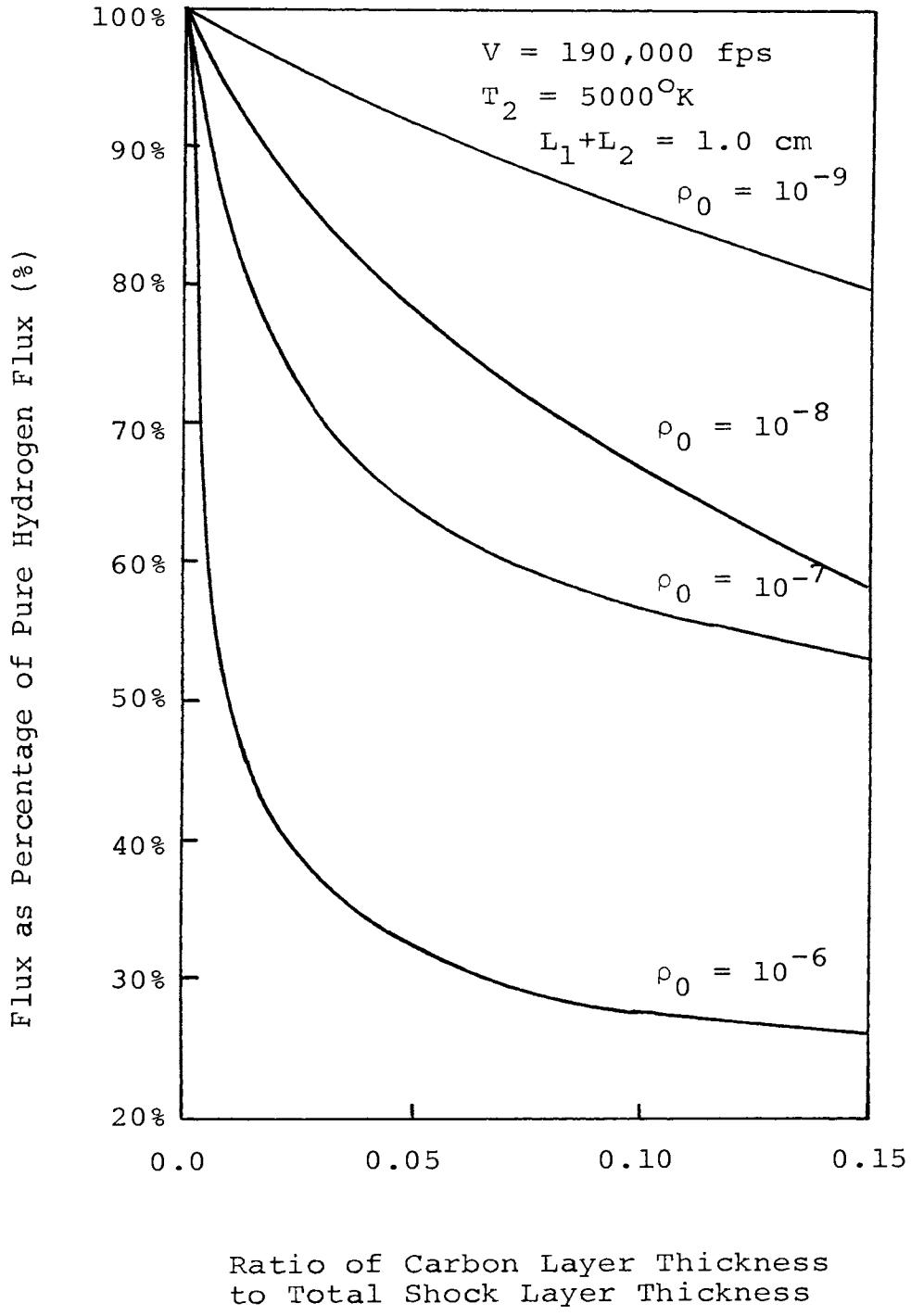

FIGURE 10. PERCENTAGE CHANGE IN FLUX I

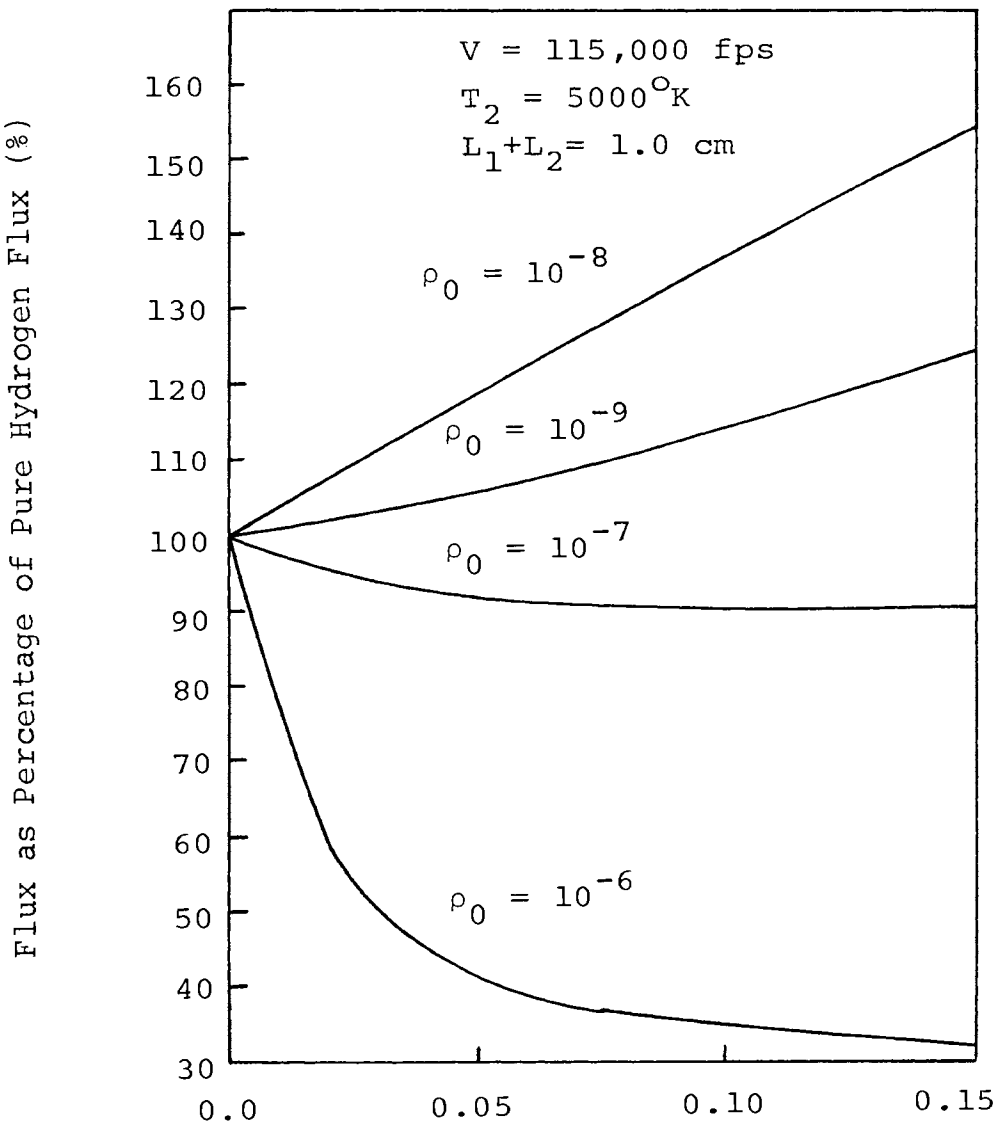

FIGURE 11. PERCENTAGE CHANGE IN FLUX II

increases and it more effectively reduces the radiation flux. As the ratio of ablation layer to hydrogen layer thickness increases for the low density case, one observes that the flux reduction is almost directly proportional to the ablation layer thickness, thus the shock layer is near its optically thin limit. As the density increases one observes that the carbon layer becomes optically thick, since increasing the ratio of ablation layer to hydrogen layer thickness does not linearly decrease the flux.

At 115,000 feet per second the addition of ablation layer decreases the radition at high ambient densities, while at low ambient densities it actually increases the radiation to the surface. This behavior can be explained as follows:

The difference between the intensity at the surface from the hydrogen-carbon combination and that from the pure hydrogen layer is

$$I_\nu - I_{\nu h} = B_\nu(T_1)(1 - \exp(-k_\nu'^{(1)}L_1)\exp(-k_\nu'^{(2)}L_2)) + B_\nu(T_2)(1 - \exp(-k_\nu'^{(2)}L_2)) - B_\nu(T_1)(1 - \exp(-k_\nu'^{(1)}(L_1 + L_2))) \qquad (5\text{-}1)$$

If the difference $(I_\nu - I_{\nu h})$ is positive, the spectral intensity at that frequency increases due to addition of the carbon layer. This occurs when $k_\nu'^{(2)}$ is large and $k_\nu'^{(1)}$ is small (hydrogen layer is optically thin) in the spectral

range where $B_\nu(T_2)$ is near its maxima. In this case Equation (5-1) reduces to

$$I_\nu - I_{\nu h} \simeq B_\nu(T_z) - B_\nu(T_1)(k'^{(2)}_\nu (L_1+L_2)) . \quad (5\text{-}2)$$

For the 115,000 fps velocity case and ambient densities of 10^{-8} and 10^{-9} gm/cm^3 this occurs in the spectral region where the carbon bands are located (2 - 8 ev). This can be seen in Figure 12, which shows the spectral distribution of radiative flux to the surface at an ambient density of 10^{-8} gm/cm^3. In some spectral regions the flux decreases slightly, but the overall effect of the ablation layer is to increase the total flux.

One can easily see from the Figure 12 that the hydrogen layer is optically thin over most of the spectrum. One would not expect the ablation layer to increase the flux if the hydrogen layer is optically thick, because of the large difference in the source functions of the two layers. In the limit when the both layers become optically thick, the Equation (5-1) reduces to

$$I_\nu - I_{\nu h} \simeq B_\nu(T_2) - B_\nu(T_1), \quad (5\text{-}3)$$

so, the flux will decrease due to addition of ablation layer.

These trends agree with those reported by Wilson[11], since he stated that in some cases the ablation layer increased

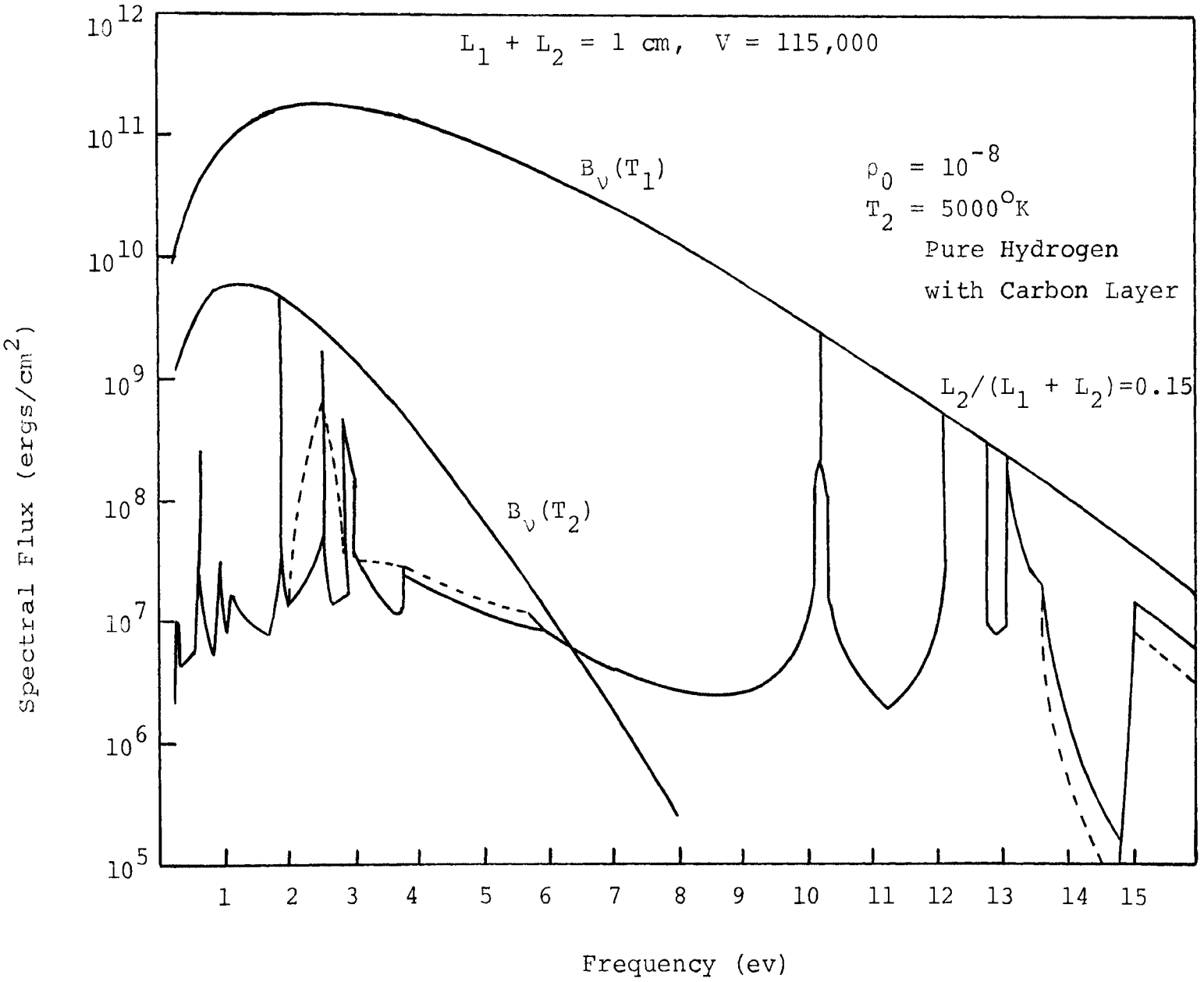

FIGURE 12. SPECTRAL FLUX DISTRIBUTION I

the radiation to the surface; however, he did not report any of the details.

B. The Influence of Carbon Lines in Reducing the Flux from Hydrogen Lines

At both velocities considered in this study the carbon lines (including C_2 bands) effectively reduce the flux to the surface from the hydrogen lines at large ambient densities, while at low densities they slightly increase the flux. At low densities the carbon bands increase the flux reaching the surface, because they appear in a portion of spectrum where the hydrogen lines are optically thin.

The carbon lines are ineffective at reducing or increasing the flux because of their small half-widths. The carbon ion lines are unimportant because of the low population of ionized carbon.

As the ambient density increases, the hydrogen lines as well as the carbon bands become optically thick. Hence, the bands readily attenuate the hydrogen line flux. This occurs mainly in the Balmer region.

Figure 13 shows that the flux due to line-line combination is small compared to the total flux at high densities, but at low densities the line-line flux and total flux are of the same order. This result is in agreement with the results of Nelson and Goulard[1]. They showed that line radiation increases in importance as the density decreases, because more lines exist at low densities.

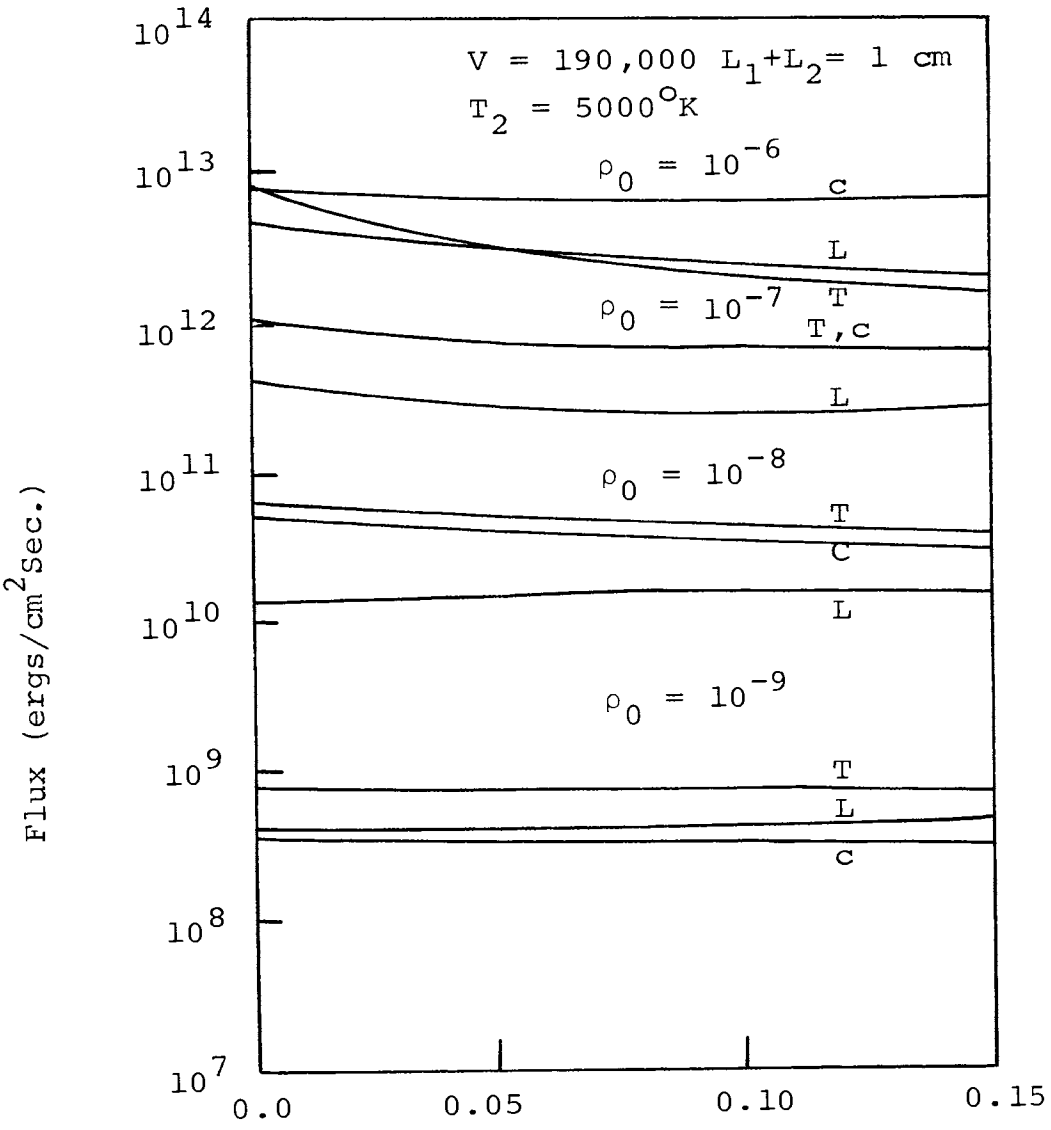

FIGURE 13. FLUX FROM SHOCK LAYER

C. The Influence of the Carbon Continuum in Reducing the Radiation from Hydrogen Continuum

The carbon continuum effectively reduces the flux to the surface from hydrogen continuum at all the densities and velocities considered in the study. Atomic carbon is the most effective ablation layer specie. The maximum flux reduction occurs in spectral range 11 - 20 ev where the atomic carbon continuum cross-section is large. In this region the atomic carbon blocks almost all the flux from the hydrogen continuum. The carbon continuum is more effective in reducing the flux as the carbon layer temperature increases. As the temperature increases, the number density and the continuum cross-section of atomic carbon increase, and the carbon continuum becomes a more effective absorber. This agrees with the results of Chin[10] who reported that the carbon atom essentially blocks all the radiation in the spectral range beyond 11 ev.

The flux reaching the surface due to the continuum-continuum combination is larger than that due to line-line combination at high densities. As can be seen from Figure 13. However, at low densities the opposite is true. This follows the trends reported by Nelson and Goulard in that the relative importance of continuum radiation increases with density.

D. The Influence of the Carbon Continuum in Reducing the Radiation from the Hydrogen Lines

The carbon continuum attenuates the flux from hydrogen lines at all the densities and velocities considered. This is due almost entirely to the continuum of atomic carbon, since for the ablation layer thermodynamic conditions considered in this study the carbon can never become important. As the number density of atomic carbon increases, it becomes more effective in reducing the flux from the hydrogen lines.

E. The Influence of the Total Shock Layer Thickness

Figures 14 and 15 show the effects of changing the total shock layer thickness. The reduction in the flux by the carbon layer increases as the total shock layer thickness increases. This reduction can be explained by looking at Figures 16 and 17, which show the spectral distribution of flux for shock layer thicknesses of 1 and 10 cm respectively, for velocity of 190,000 fps and ambient density of 10^{-7} gm/cm^3. For both thicknesses the carbon layer absorbs essentially all the radiation from hydrogen layer in the spectral region 11 - 20 ev. This absorption is due to the presence of the atomic carbon. The reduction in the spectral region from 2 - 8 is due to the carbon bands.

For the pure hydrogen shock layer, Figure 14 shows that the flux increases with shock layer thickness; however, the shock layer is not optically thin since the flux does not increase in direct proportion to the thickness. If

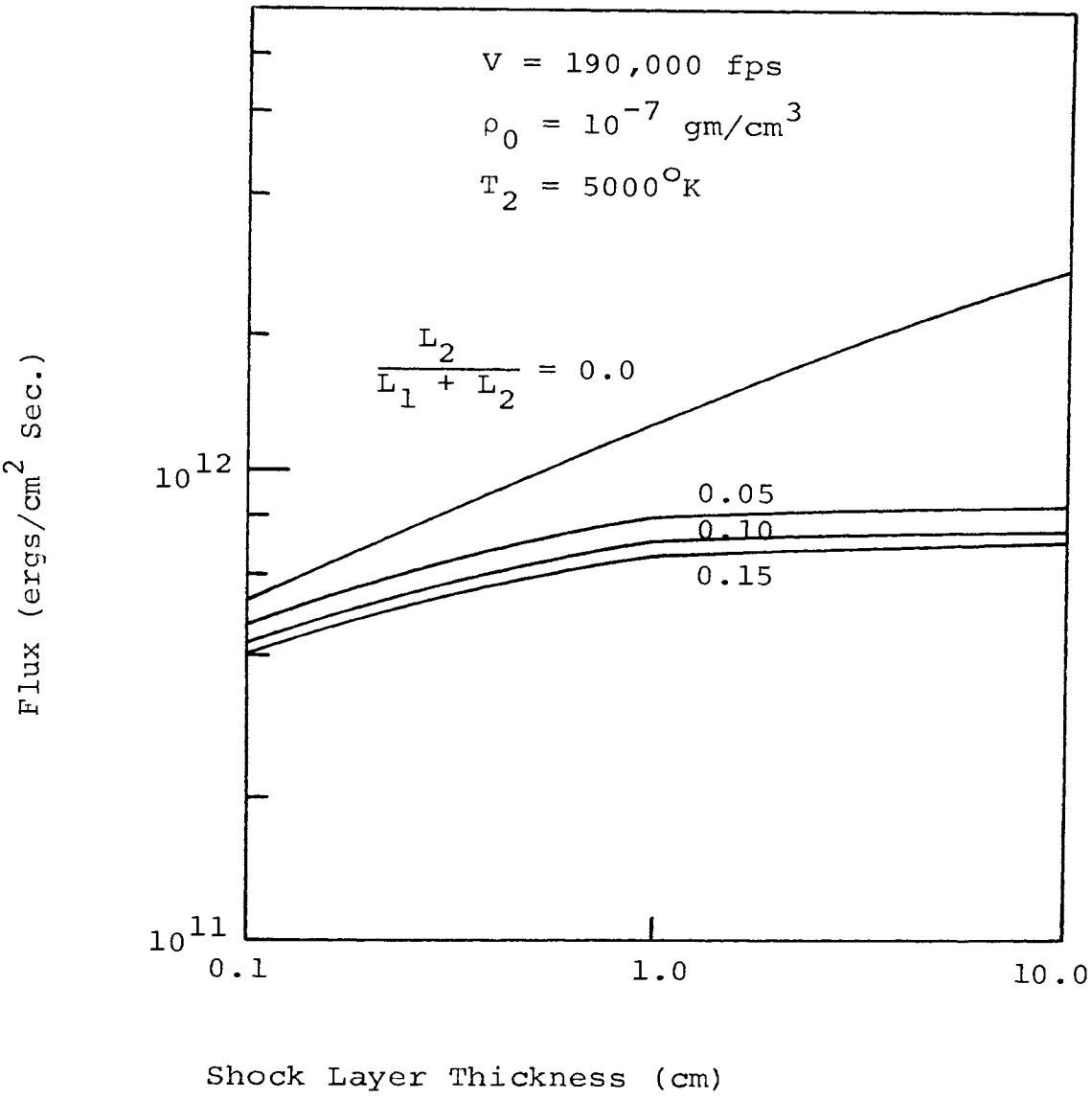

FIGURE 14. FLUX FOR DIFFERENT SHOCK LAYER THICKNESS

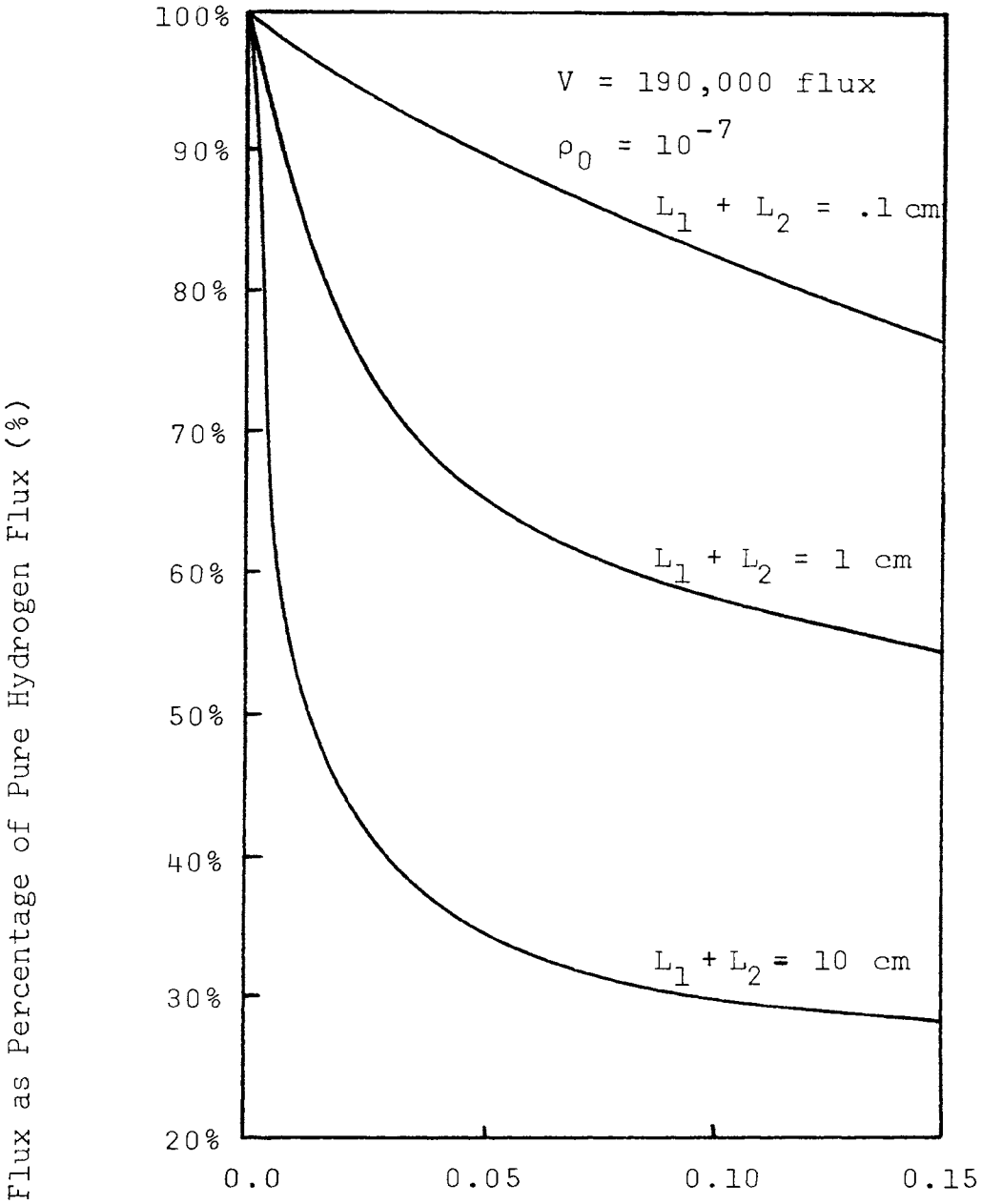

FIGURE 15. CHANGE IN FLUX WITH CARBON LAYER THICKNESS

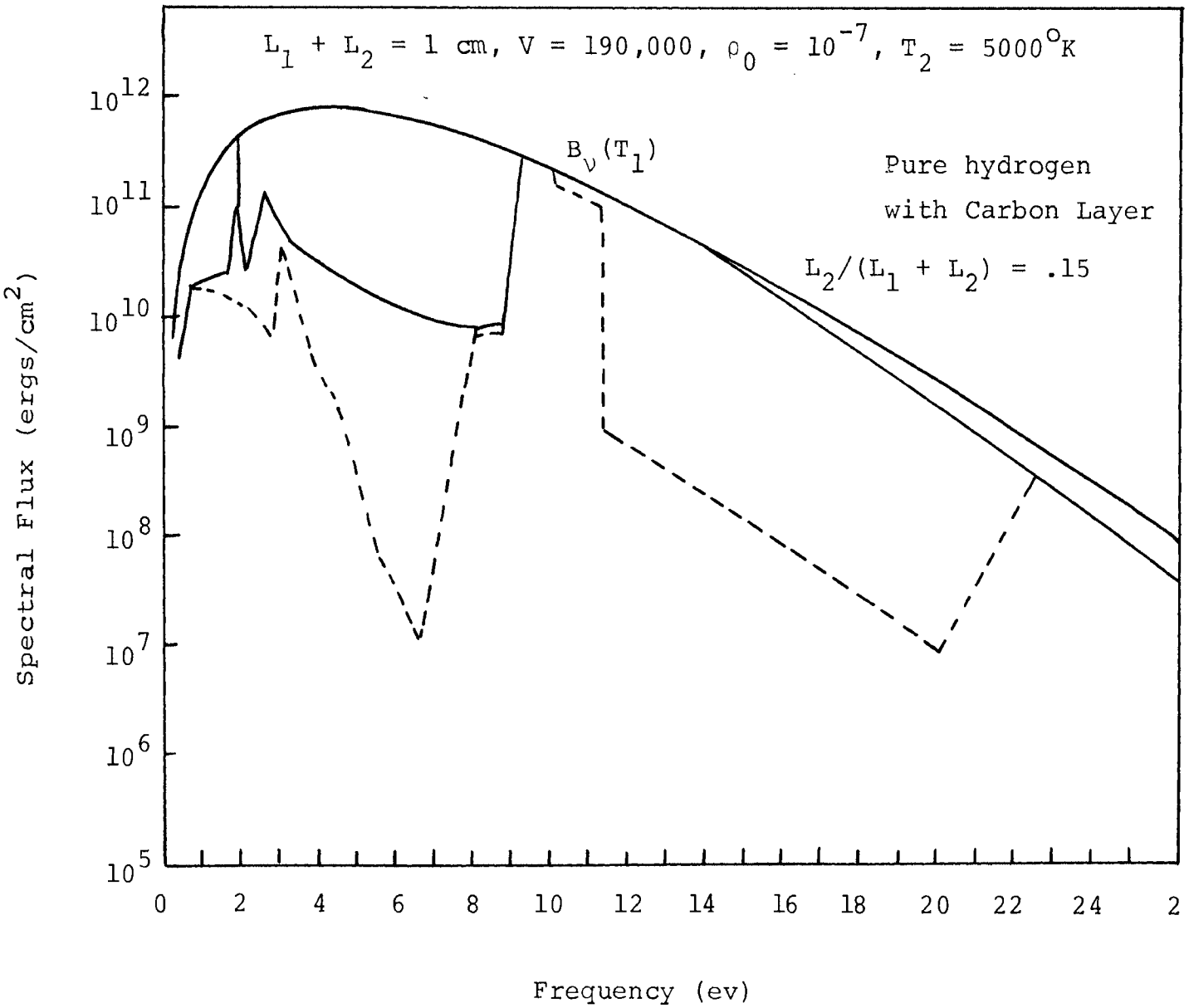

FIGURE 16. SPECTRAL FLUX DISTRIBUTION II

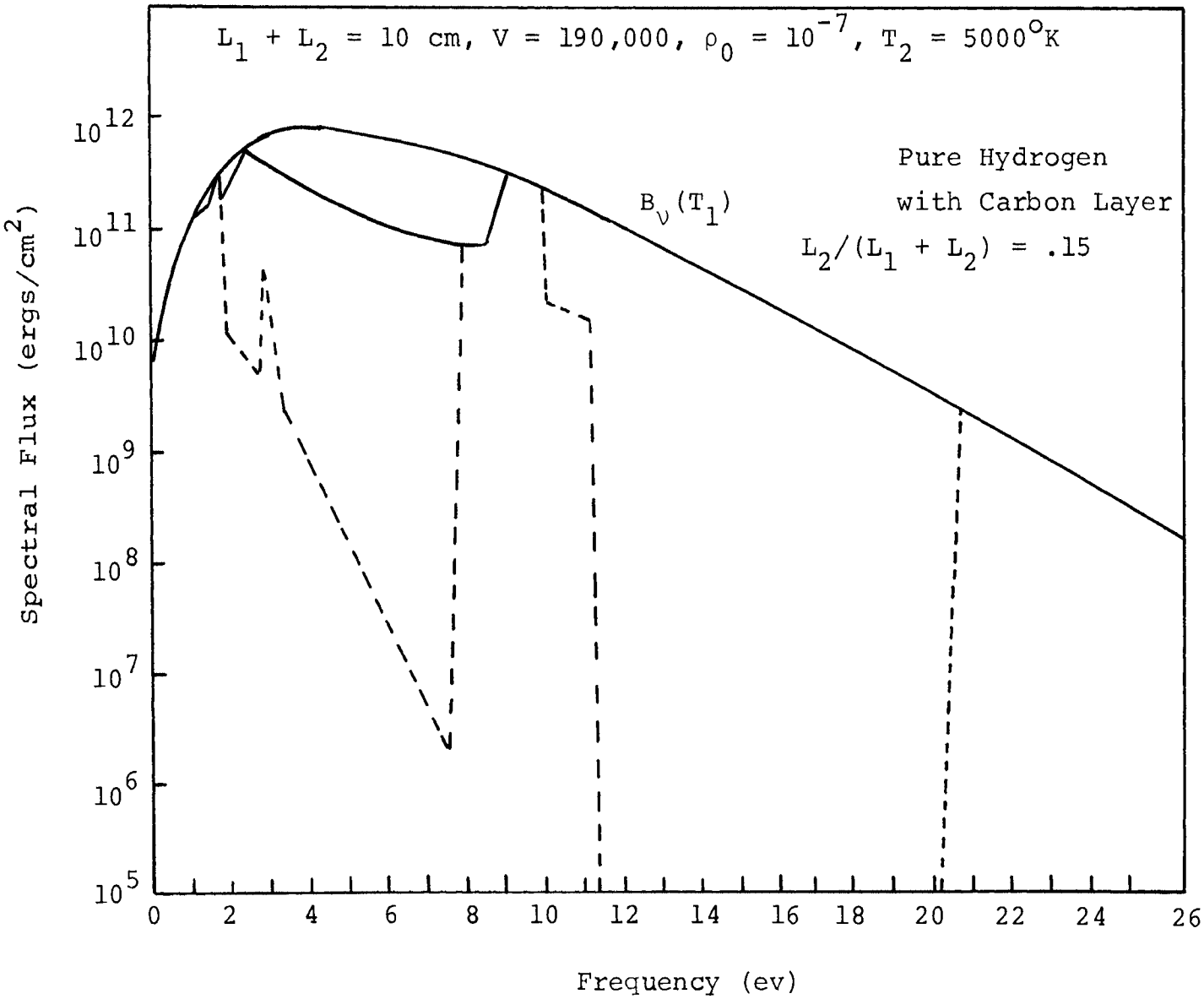

FIGURE 17. SPECTRAL FLUX DISTRIBUTION III

the shock layer were optically thick,the flux would remain constant as the thickness increased. When the ablation layer us added, the shock layer appears to be almost optically thick. This is because the molecular bands and atomic carbon continuum strongly attenuate the radiation in their respective spectral regions, once the ablation layer thickness becomes greater than almost one-half a centimeter.

F. The Influence of the Ablation Layer Temperature

Figure 18 shows results for different carbon layer temperatures (3000, 5000 and 7000^{o}K) at a velocity of 190,000 fps and ambient density of 10^{-7} gm/cm^{3}. The flux to the surface increases as the carbon layer temperature decreases. When the carbon layer temperature is 3000^{o}K, the number density of molecular carbon is very high compared to that of atomic carbon. Thus, molecular carbon is essentially the only carbon specie available to attenuate the radiation. Figure 19 shows the spectral distribution of the flux for an ablation layer temperature of 3000^{o}K. Note that the flux is greatly reduced in the region 2 - 7 ev where the carbon bands are located, while in the other spectral regions the ablation layer hardly influences the flux. This behavior is because the population of C and C^{+} is very small at this pressure and temperature.

At an ablation layer temperature of 5000^{o}K (see Figure 16), the reduction in flux occurs mainly in the spectral

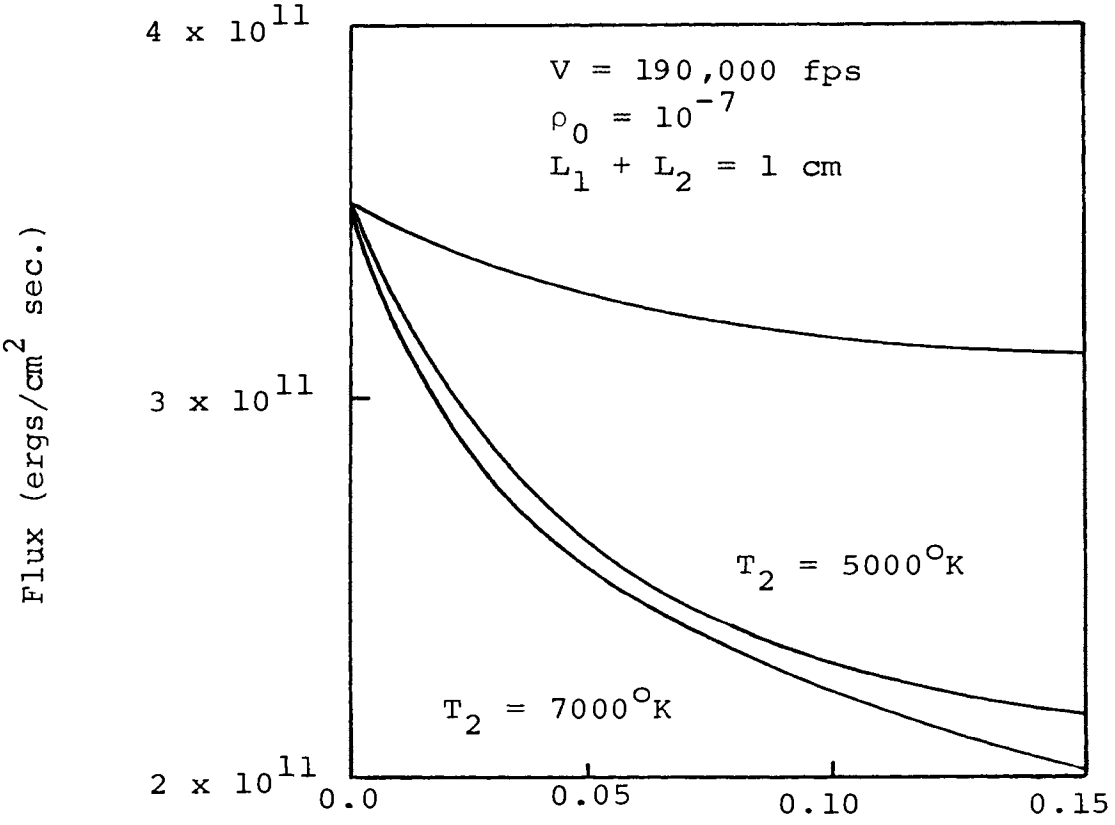

FIGURE 18. EFFECT OF CARBON LAYER TEMPERATURE ON FLUX

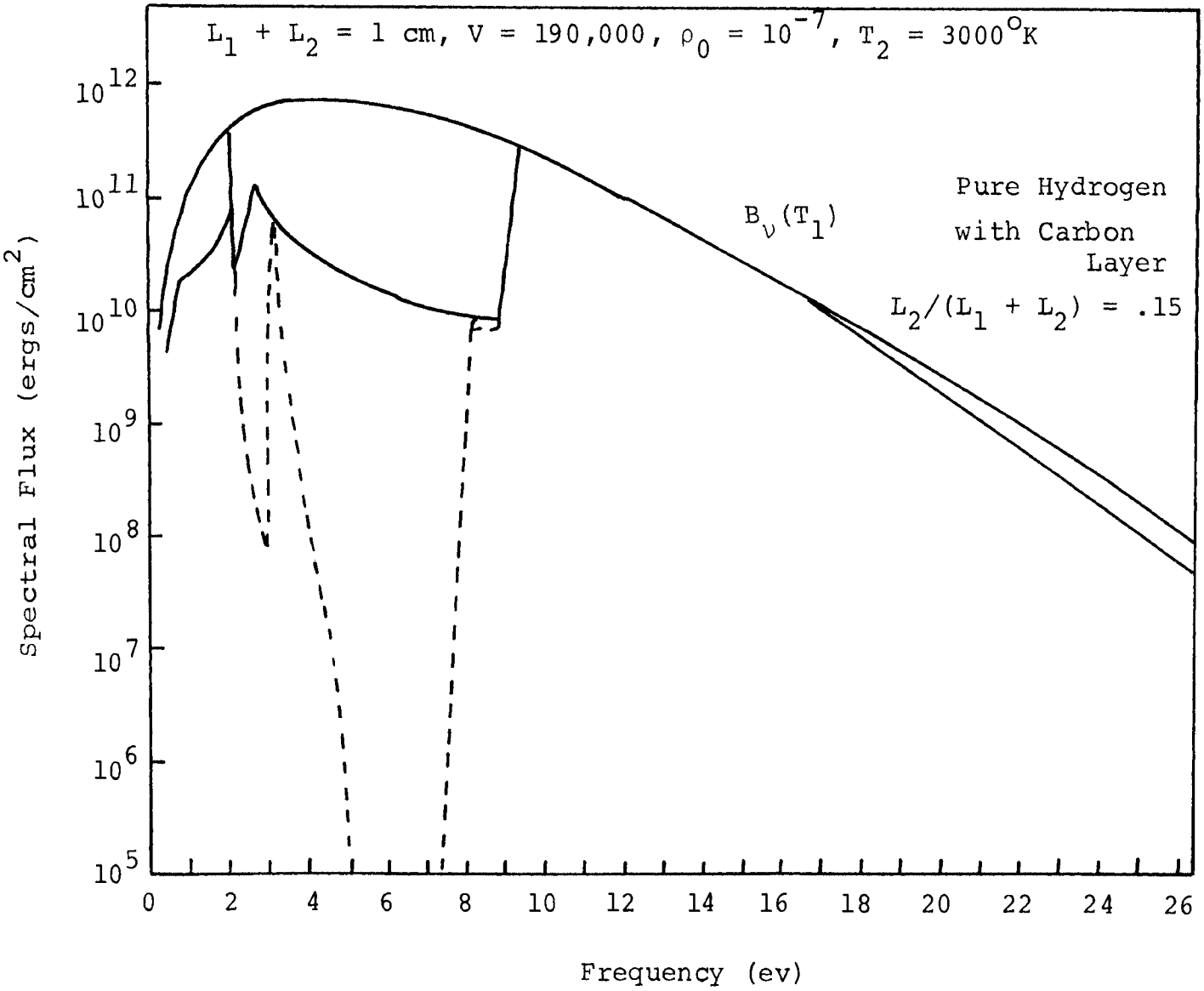

FIGURE 19. SPECTRAL FLUX DISTRIBUTION IV

regions from 2 - 8 ev and 11 - 20 ev. The reduction in the first region is due to carbon bands and in the second due to the atomic carbon. Although the reduction in the flux in the region 2 - 8 ev is small as compared to that of $3000^{o}K$ ablation layer case, the large reduction in the 11 - 20 ev region increases reduction of the total flux.

Figure 20 shows the spectral distribution of flux at an ablation layer temperature of $7000^{o}K$. The maximum reduction in flux occurs in the spectral range 11 - 20 ev, because at $7000^{o}K$ the number density of atomic carbon is large and it becomes the main absorber in the ablation layer. Although the reduction in flux due to carbon bands is very small, the large reduction due to the atomic carbon reduces the total flux to below its value at an ablation layer temperature of $5000^{o}K$.

These trends agree with those reported by Hoshizaki and Lasher[9]. They found that atomic carbon was generally the most important ablation layer specie, but that molecular carbon became important for some conditions.

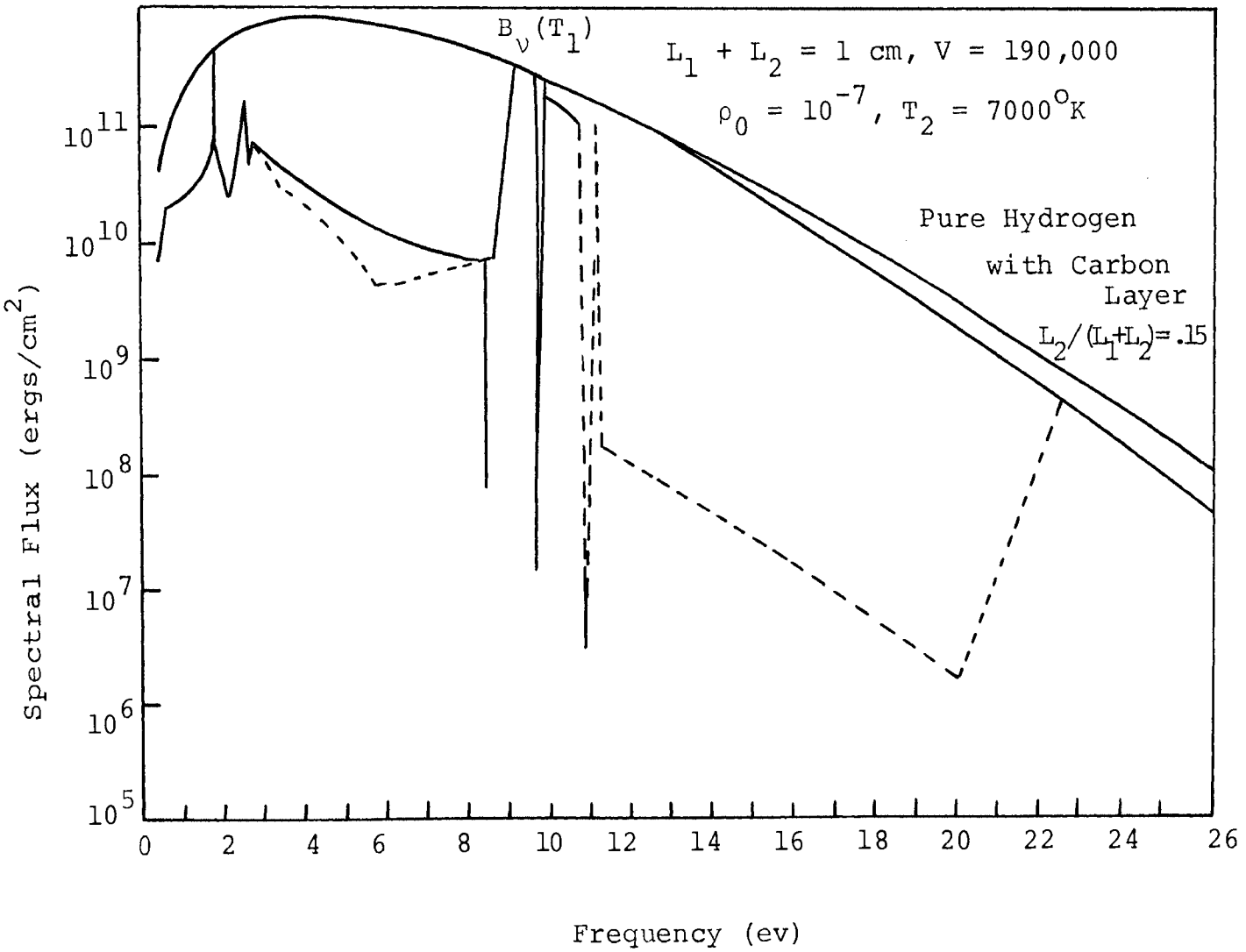

FIGURE 20. SPECTRAL FLUX DISTRIBUTION V

VI. SUMMARY AND CONCLUSIONS

A simplified model is developed to study the effect of ablation layers on the radiation from equilibrium hydrogen plasmas at conditions similar to those expected in entry to the atmosphere of Jupiter. The shock layer model is assumed to consist of two plane parallel layers; one consisting of hydrogen, and the other of carbon species. Each layer is assumed to be in thermodynamic equilibrium at its respective temperature. The thermodynamic conditions in the hydrogen portion of the layer are arrived at by solving the Rankine-Hugoniot Equations across the shock. The temperature of the carbon layer is taken as a parameter in the problem, and the values investigated (3000, 5000 and 7000^{o}K) are intended to cover the range of possible surface temperatures. Two entry velocities (115,000 and 190,000 fps) and four ambient densities (10^{-6} through 10^{-9} gm/cm^{3}) are considered. Total shock layer thickness is allowed to vary from .1 to 10 cm. The following conclusions can be drawn from this study:

1) The addition of carbon ablation layer reduces the flux reaching the surface due to the hydrogen layer in most cases, but not always. The reduction increases as the density and velocity increase. The ablation layer increases the flux

when the hydrogen layer is optically thin and the ablation layer is optically thick.

2) Atomic carbon is the most effective absorber in the carbon layer. Molecular carbon bands also become very important as the ambient density and temperature decrease.

3) The atomic and ionic carbon lines are unimportant in reducing the flux from the hydrogen layer because their half-widths are small. Also, the number density of ionized carbon is also very small at the temperatures considered.

4) The carbon layer becomes more effective in reducing the flux from the hydrogen layer when the ablation layer thickness is increased, because the C_2 bands and atomic carbon continuum become optically thick.

VII. APPENDICES

Appendix A. Rankine-Hugoniot Equations

The Rankine-Hugoniot Equations which relate the variables of state on either side of a shock front, are[16]

$$\rho_0 V_0 = \rho_1 V_1 \tag{A-1}$$

$$P_0 + \rho_0 V_0^2 = P_1 + \rho_1 V_1^2 \tag{A-2}$$

$$i_0 + 1/2 V_0^2 = i_1 + 1/2 V_1^2 \tag{A-3}$$

where V is the gas velocity component normal to, and with respect to the shock. The subscripts 0 and 1 label the quantities in front of and behind the shock.

For a strong shock $\rho_0 V_0^2 >> P_0$ and $V_0^2 >> i_0$; therefore, i_0 and P_0 can be neglected. The enthalpy behind the shock is

$$i_0 = \frac{kT_1^2}{\rho_1} \Sigma \frac{N_i}{Z_i} \frac{\delta Z_i}{\delta T_i} + \frac{P_1}{\rho_1} , \tag{A-4}$$

and the pressure behind the shock is

$$P_1 = kT \Sigma_i N_i \tag{A-5}$$

Appendix B. Partition Function

A. Electronic

1. Atomic Carbon

The electronic partition function for atomic carbon is[3]

$$Q_c = \sum_n g_n \exp\left(-\frac{E_n}{kT}\right) \qquad \text{(B-1)}$$

where g_n is the statistical weight and E_n is the energy of the n^{th} level of atomic carbon. The values of g_n and E_n are taken from Gilmore[13], and are given in Table B I.

2. Singly Ionized Carbon

The electronic partition function for singly ionized carbon is obtained from Equation (B-1) using the current values of g_n and E_n. These are tabulated in Table B II.

3. Atomic Hydrogen

The electronic partition function for atomic hydrogen is given by Equation (B-1) where

$$g_n = 2n^2 \qquad \text{(B-2a)}$$

and

$$E_n = I^*_H\left(1 - \frac{1}{n^2}\right) \qquad \text{(B-2b)}$$

I^*_H is the ionization limit of atomic hydrogen. The sum is truncated to include only levels whose energies are below the reduced ionization limit.

The reduction in ionization potential of a hydrogen atom due to surrounding plasma is[7]

$$\Delta I_H = \frac{e^2}{\rho_D} \tag{B-4}$$

where the Debye radius is defined as

$$\rho_D = \left[\frac{kT}{4\pi\ e^2 [\sum_i z_c^2\ N_i]}\right]^{1/2} \tag{B-5}$$

4. Protons and Electrons

The electronic partition functions for protons and electrons are[5]

$$Q_P = 1 \tag{B-6}$$

$$Q_e = 2 \tag{B-7}$$

B. Translational

The translational partition function for any particle of mass m is given by[16]

$$Q^t = \left[\frac{2\pi mkT}{h^2}\right]^{3/2} \tag{B-8}$$

in units of cm^{-3}

C. Molecular Hydrogen (H_2)

The partition function of molecular hydrogen is written as

$$Z_{H_2} = Q_{H_2}^{(tr)}\ Q_{H_2}(int) \tag{B-9}$$

where $Q_{H_2}^{(tr)}$ represents the translational partition function. The internal partition function is represented by $Q_{H_2}(int)$ and is taken from Table 5, Page 39, Rosenbaum and Levitt[23].

D. Molecular Hydrogen Ion

The partition function of molecular hydrogen ion is written as

$$Z_{H_2}^{+} = Q_{H_2}(tr)\ Q_{H_2}(int)\ \exp\left[\frac{D - I_H - D'}{kT}\right] \quad \text{(B-10)}$$

where $Q_{H_2}(int)$ is the internal partition function and is taken from Table II, pp. 61 of Patch and McBride[24]. The energy relative to that of H is represented by the exponential where

$$D = 36113.3 \quad cm^{-1}$$
$$I_H = 109678.8 \quad cm^{-1}$$
$$D = 21379.4 \quad cm^{-1}$$

and they represent respectively the dissociation energy of H_2, the ionization energy of H and the dissociation energy of H_2^{+}[26]

E. Negative Hydrogen Ion (H^-)

The partition function for the negative hydrogen ion is written as

$$Z_{H^-} = Q_{H^-}^{(tr)}\ \exp\frac{-I_{H^-}}{kT} \quad \text{(B-11)}$$

where I_{H^-} is the ionization energy (6218.7 cm^{-1}) of the negative hydrogen.

F. Free Energies

1. Molecular Carbon (C_2);

The free energies for molecular carbon are taken from Fickett and Cowan[14]. Curve fits of enthalpy and entropy are given in their work and the expressions are given in their work and the expressions are listed below.

$$(H^0 - H_0^0)/RT = a + bT + cT^2 + dT^3 \qquad \text{(B-12)}$$

$$S^0/R = a \ln T + 2bT + 3/2\ cT^2 + 4/3\ dT^3 + e \qquad \text{(B-13)}$$

where

$a = 3.85829$

$b = 1.37009 \times 10^{-4}$

$c = -.86238 \times 10^{-8}$

$d = .33821 \times 10^{-12}$

$e = 2.61129$

2. Atomic carbon(C);

The free energy expression for atomic carbon is given by[13]

$$-\left(\frac{F_T^0 - E_0^0}{RT}\right) = \ln (Q_C) + 2.5 \ln T + 1.5 \ln(M) - 3.66496 \qquad \text{(B-14)}$$

where M is the atomic weight of carbon atom.

Table B I. Atomic Carbon Partition Functions

n	g_n	E_n(ev)
2	1	0.0
2	3	0.0020
2	5	0.0054
2	5	1.2639
2	1	2.6839
2	5	4.1825
3	12	7.5351
2	15	7.9461
3	36	8.6442
2	9	9.3303
4	12	9.6933
3	60	9.7233
4	36	10.0258
4	60	10.3958
4	84	10.4144
3	5	12.1350

Table B II. Partition Functions for Singly Ionized Carbon

n	g_n	E_n (ev)
2	2	0.0
2	4	0.0079
2	12	5.3353
2	10	9.2901
2	2	11.9634
2	6	13.7189

Appendix C. Absorption Coefficients

A. Continuum Absorption Cross-Sections for Neutral Carbon

The values of absorption cross-sections for neutral carbon are taken from Wilson and Nicolet[18] and the curve fit equations are listed below.

Group 1. $0 \leq h\nu \leq 3.78$ ev

$$\sigma_c = \frac{6.26 \times 10^{-20} \Gamma_k T z_k^2 e^{-(I_c - h\nu)} \xi_k(h\nu)}{(h\nu)^3} \quad \text{(C-1)}$$

where $\Gamma_k = 2Q_k^{z+1}/Q_k^z$, Q_k^{Z+1} is the electronic partition function of the residue ion and Q_k^z is the electronic partition function of the parent atom, ξ_k is a quantum mechanical correction factor which has been calculated by Biberman[17]. Figure (21) shows ξ_k as a function of frequency. I_c is the ionization potential of carbon (11.264 ev).

Group 2. $3.78 < h\nu \leq 8.510$ ev

$$\sigma_c = \frac{6.26 \times 10^{-20} \Gamma_k T z_k^2 e^{-(I_c - 3.78)} \xi_k(h\nu)}{(h\nu)^3} \quad \text{(C-2)}$$

$$\xi_c(h\nu) = 1 - .4053(h\nu) + .0587(h\nu)^2 \quad \text{(C-2a)}$$

Group 3. $8.510 < h\nu \leq 10.0$ ev

$$\text{Log}(\sigma_c) = -17.6396 - 14.4229(1000/T) + 2.48902$$

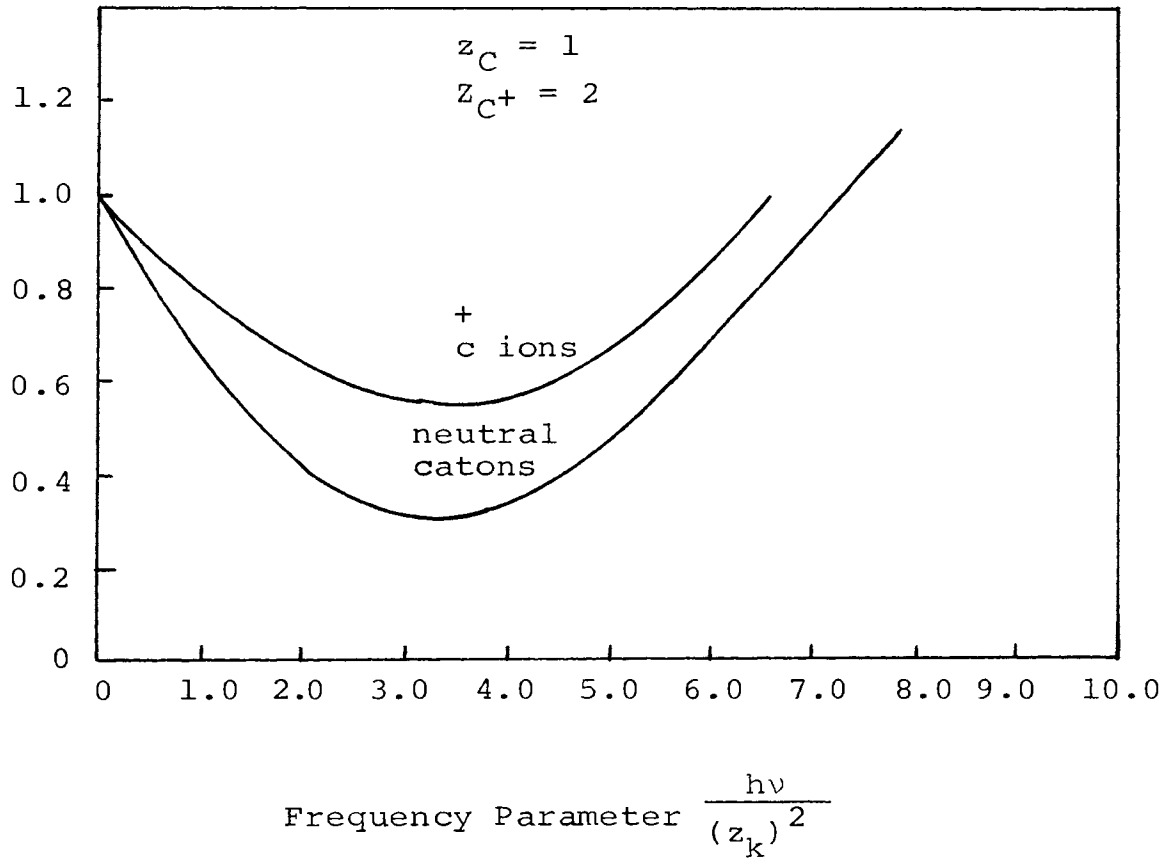

FIGURE 21. QUANTUM-MECHANICAL CORRECTION FACTOR $\xi(h\nu)$

$$(10^6/T^2) + .0484(10^9/T^3) - .01529(10^{12}/T^4$$

$$+ .5948(10^{12}/T^5) - .8645(10^{13}/T^6) \qquad \text{(C-3)}$$

Group 4. $10.0 < h\nu \leq 11.26$ ev

$$\text{Log}(\sigma_C) = -16.857 - 10.5628(1000/T) + 9.4482$$
$$(10^6/T^2) + 220.938(10^9/T^3) - 1162/38$$
$$(10^{12}/T^4) + 594.637\ (10^{15}/T^5) + 2841.57$$
$$(10^{18}/T^6) \qquad \text{(C-4)}$$

Group 5. $11.26 < h\nu \leq 20$ ev

$$\sigma_C = 10^{-17}\ [9.9 + 8.5\ e^{-1.26/kT} + 2.2\ e^{-2.75/kT}$$
$$+ 5\ e^{-4.18/kT}] / 9 + e^{-2.68/kT} + 5$$
$$\{e^{-1.265/kT} + e^{-4.18/kT}\} \qquad \text{(C-5)}$$

B. Continuum Absorption Cross-Section for Singly Ionized Carbon

The continuum absorption cross-section for singly ionized carbon are also taken from Wilson and Nicolet[18], and curve fit equations are listed below.

Group 1. $0 < h\nu \leq 15$ ev

$$\sigma_{C^+} = \frac{6.26 \times 10^{-20}\ \Gamma_{C^+}\ Tz_{C^+}^2\ e^{-(I_{C^+} - h\nu)}\ \xi_{C^+}(h\nu)}{(h\nu)^3} \qquad \text{(C-6)}$$

$$\xi_{C^+}(h\nu) = 1 - .2647(h\nu/4) + .0378(h\nu/4)^2 \qquad \text{(C-7)}$$

where I_{C^+} is the ionization potential of singly ionized carbon (24.376 ev)

Group 2. $15.0 < h\nu < 19.0$ ev

$$\text{Log}(\sigma_{C^+}) = -\frac{Y_1 - Y_2}{4} h\nu - \frac{(15Y_2 - 19Y_1)}{4} \quad \text{(C-8)}$$

where $Y_1 = \text{Log}\left[6.26 \times 10^{-26} \times 8 \frac{Q_{C^{++}}}{Q_{C^+}} \frac{T}{(h\nu)^3} \xi_{C^+} e^{(-9.376/kT)}\right]$ (C-9)

$$Y_2 = -18.7307 - 47.6461(1000/T - 70.6488(10^6/1T^2) + 474.521(10^9/T^3) - 863.097\ (10^{12}/T^4) - 1216.08\ (10^{15}/T^5) + 3821.04\ (10^{18}/T^6) \quad \text{(C-10)}$$

Group 3. $19 < h\nu \leq 20$ ev

$$\text{Log}\ (\sigma_{C^+}) = -17.0472 - 22.1653\ (1000/T) - 71.41\ (10^6/T^2) + 420.29\ (10^9/T^3) - 831.05\ (10^{12}/T^4) - 636.485\ (10^{15}/T^5) + 2734.74\ (10^{18}/T^6) \quad \text{(C-11)}$$

C. Absorption Cross-Sections for Molecular Carbon Bands

The absorption cross-sections for the carbon bands are treated in an approximate fashion. Absorption cross-section for each band was fitted to the values given in reference 9. The band averaged absorption cross-sections are listed below.

1) Swan $2 < h\nu < 3$ ev

$$\text{Log } \sigma = -5.9088\ (h\nu - 2.5)^2 - 16.5228 \qquad \text{(C-12)}$$

2) Mulliken $5.25 < h\nu < 6.05$ ev

$$\text{Log } \sigma = -15.48\ (h\nu - 5.65)^2 - 16.5228 \qquad \text{(C-13)}$$

3) Freymark $4.0 < h\nu < 8$ ev

$$\text{Log } \sigma = -.444\ (h\nu - 6)^2 - 16.5228 \qquad \text{(C-14)}$$

4) Fox Herzberg $2.75 < h\nu < 5.25$ ev

$$\text{Log } \sigma = -1.02\ (h\nu - 4)^2 - 17.398 \qquad \text{(C-15)}$$

D. The Negative Hydrogen Ion

The absorption cross-section for the negative hydrogen is taken from Darwin and Felenbok[22], and is given in Table C I.

E. The Molecular Hydrogen Ion

The absorption coefficient for the molecular hydrogen is taken from Boggess[21]. The emission coefficient per neutral hydrogen atom H^{O} and per proton H^{+}, $F(\lambda,T)$ is given by the relation

$$\text{Log } F(\lambda, T) = C(\lambda) - \frac{D(\lambda)}{T} \qquad \text{(C-16)}$$

where $C(\lambda)$ and $D(\lambda)$ are special numerical values. These are given by Boggess[21].

Table C I. H^- Absorption Cross-Sections

$\lambda(A^o)$	$\sigma(\lambda) \cdot 10^{17} cm^2$
13995	1.50
12131	2.96
10111	4.13
9102	4.44
8669	4.50
8275	4.52
7283	4.41
6280	4.06
5875	3.87
5059	3.39
4443	2.97
3960	2.62
3572	2.32
2987	1.84
2249	1.231
1642	0.740
1066	0.333
505	0.0657

Appendix D. Tabulated Results

The data obtained from the results are tabulated in Tables D I through D XII. The notations used in these tables are as follows:

C	=	velocity (feet per second).
ρ_1	=	density in the hydrogen layer (gm/cm^3).
T_1	=	temperature of the hydrogen layer (^oK).
T_2	=	temperature of the carbon layer (^oK).
P	=	pressure in the shock layer (atm.).
T-T flux	=	total flux reaching the surface ($ergs/cm^2sec$).
L-L flux	=	flux due to the line-line combination (including c_2 bands).
C-C flux	=	flux due to the continuum-continuum combination.
HL-CC flux	=	flux due to the combination of hydrogen lines and carbon (continuum).
T-T Int.	=	total intensity reaching the surface ($ergs/cm^2sr.$).
L-L Int.	=	intensity due to the line-line combination (including c_2 bands).
C-C Int.	=	intensity due to the continuum-continuum combination.
HL-CC Int.	=	intensity due to the combination of hydrogen lines and carbon continuum.

Table D I. Results ($V = 190{,}000$, $\rho_1 = 1.086.10^{-5}$, $\rho_0 = 10^{-6}$, $T_1 = 21{,}380$, $T_2 = 5000$, $P = 30.825$)

	$L_1 = 1.0$ $L_2 = 0.0$	$L_1 = .95$ $L_2 = .05$	$L_1 = .90$ $L_2 = .10$	$L_1 = .85$ $L_2 = .15$
T.T. Flux	9.36 E12	2.90 E12	2.67 E12	2.56 E12
L.L. Flux	5.07 E12	3.07 E12	3.01 E12	2.95 E12
C.C. Flux	8.75 E12	6.92 E12	6.66 E12	6.45 E12
HL-CC Flux		3.61 E12	3.36 E12	3.16 E12
T.T. Int.	2.66 E12	9.69 E11	8.89 E11	8.47 E11
L.L. Int.	1.25 E12	8.48 E11	8.23 E11	8.04 E11
C.C. Int.	2.49 E12	1.94 E12	1.87 E12	1.81 E12
HL-CC Int.		8.63 E11	7.99 E11	7.45 E11

Table D II. Results ($V = 190{,}000$, $\rho_1 = 1.261.10^{-6}$, $\rho_0 = 10^{-7}$, $T_1 = 17{,}957$, $T_2 = 5000$, $P = 3.0868$)

	$L_1 = 1.0$ $L_2 = 0.0$	$L_1 = .95$ $L_2 = .05$	$L_1 = .90$ $L_2 = .10$	$L_1 = .85$ $L_2 = .15$
T.T. Flux	1.24 E12	7.95 E11	7.12 E11	6.74 E11
L.L. Flux	3.38 E11	2.88 E11	2.75 E11	2.66 E11
C.C. Flux	1.14 E12	8.15 E11	7.47 E11	7.13 E11
HL-CC Flux		2.03 E11	1.75 E11	1.60 E11
T.T. Int.	3.49 E11	2.56 E11	2.27 E11	2.14 E11
L.L. Int.	7.51 E10	6.82 E10	6.53 E10	6.28 E10
C.C. Int.	3.30 E11	2.52 E11	2.26 E11	2.15 E11
HL-CC Int.		4.80 E10	3.89 E10	3.49 E10

Table D III. Results ($V = 190{,}000$, $\rho_1 = 1.452.10^{-7}$, $\rho_0 = 10^{-8}$, $T_1 = 15{,}272$, $T_2 = 5000$, $P = 3.101.10^{-1}$

	$L_1 = 1.0$ $L_2 = 0.0$	$L_1 = .95$ $L_2 = .05$	$L_1 = .90$ $L_2 = .10$	$L_1 = .85$ $L_2 = .15$
T.T. Flux	6.07 E10	4.79 E10	4.06 E10	3.56 E10
L.L. Flux	1.27 E10	1.28 E10	1.28 E10	1.28 E10
C.C. Flux	5.03 E10	3.88 E10	3.21 E10	2.76 E10
HL-CC Flux		1.00 E10	8.47 E09	7.41 E09
T.T. Int.	1.21 E10	1.10 E10	9.70 E09	8.65 E09
L.L. Int.	2.68 E09	2.7 E09	2.71 E09	2.71 E09
C.C. Int.	1.01 E10	8.73 E09	7.58 E09	6.63 E09
HL-CC Int.		2.34 E09	2.07 E09	1.84 E09

Table D IV. Results ($V = 190{,}000$, $\rho_1 = 1.652.10^{-8}$, $\rho_0 = 10^{-9}$, $T_1 = 13{,}180$, $T_2 = 5000$, $P = 3.1175.10^{-2}$)

	$L_1 = 1.0$	$L_1 = .95$	$L_1 = .90$	$L_1 = .85$
	$L_2 = 0.0$	$L_2 = .05$	$L_2 = .10$	$L_2 = .15$
T.T. Flux	7.87 E08	7.24 E08	6.73 E08	6.28 E08
L.L. Flux	3.98 E08	3.95 E08	3.91 E08	3.88 E08
C.C. Flux	3.98 E08	3.48 E08	3.07 E08	2.73 E08
HL-CC Flux		3.73 E08	3.51 E08	3.30 E08
T.T. Int.	1.36 E08	1.44 E08	1.38 E08	1.31 E08
L.L. Int.	8.56 E07	8.45 E07	8.34 E07	8.22 E07
C.C. Int.	6.57 E07	6.10 E07	5.64 E07	5.21 E07
HL-CC Int.		8.21 E07	7.86 E07	7.51 E07

Table D V. Results ($V = 115{,}000$, $\rho_1 = 9.22.10^{-6}$, $\rho_0 = 10^{-6}$, $T_1 = 13{,}395$, $T_2 = 5000$, $P = 1.023.10^{1}$)

	$L_1 = 1.0$	$L_1 = .95$	$L_1 = .90$	$L_1 = .85$
	$L_2 = 0.0$	$L_2 = .05$	$L_2 = .10$	$L_2 = .15$
T.T. Flux	3.07 E11	1.21 E11	1.06 E11	9.77 E10
L.L. Flux	2.34 E11	1.23 E11	1.16 E11	1.12 E11
C.C. Flux	9.97 E10	7.98 E10	7.55 E10	7.16 E10
HL-CC Flux		2.04 E11	1.92 E11	1.81 E11
T.T. Int.	5.50 E10	2.99 E10	2.60 E10	2.37 E10
L.L. Int.	4.81 E10	3.09 E10	2.90 E10	2.71 E10
C.C. Int.	1.93 E10	1.37 E10	1.28 E10	1.20 E10
HL-CC Int.		4.06 E10	3.80 E10	3.58 E10

Table D VI. Results ($V = 115{,}000$, $\rho_1 = 1.02 \cdot 10^{-6}$, $\rho_0 = 10^{-7}$, $T_1 = 11{,}957$, $T_2 = 5000$, $P = 1.0965$)

	$L_1 = 1.0$	$L_1 = .95$	$L_1 = .90$	$L_1 = .85$
	$L_2 = 0.0$	$L_2 = .05$	$L_2 = .10$	$L_2 = .15$
T.T. Flux	1.31 E10	1.19 E10	1.18 E10	1.18 E10
L.L. Flux	1.08 E10	1.21 E10	1.29 E10	1.33 E10
C.C. Flux	2.91 E09	1.99 E09	1.63 E09	1.43 E09
HL-CC Flux		8.90 E09	8.01 E09	7.39 E09
T.T. Int.	2.37 E09	2.80 E09	2.88 E09	2.94 E09
L.L. Int.	2.20 E09	2.71 E09	3.02 E09	3.22 E09
C.C. Int.	6.65 E09	4.61 E09	3.47 E08	2.78 E08
HL-CC Int.		1.83 E09	1.64 E09	1.49 E09

Table D VII. Results ($V = 115{,}000$, $\rho_1 = 1.142.10^{-7}$, $\rho_0 = 10^{-8}$, $T_1 = 10{,}669$, $T_2 = 5000$, $P = 1.1077.10^{-1}$)

	$L_1 = 1.0$	$L_1 = .95$	$L_1 = .90$	$L_1 = .85$
	$L_2 = 0.0$	$L_2 = .05$	$L_2 = .10$	$L_2 = .15$
T.T. Flux	4.08	4.81 E08	5.57 E08	6.34 E08
L.L. Flux	3.64 E08	4.62 E08	5.56 E08	6.46 E08
C.C. Flux	4.39 E07	3.82 E07	3.77 E07	3.01 E07
HL-CC Flux		3.32 E08	3.06 E08	2.84 E08
T.T. Int.	6.99 E07	3.54 E07	1.08 E08	1.22 E08
L.L. Int.	7.44 E07	9.01 E07	1.06 E08	1.21 E08
C.C. Int.	7.91 E06	7.20 E06	6.55 E06	5.95 E06
HL-CC Int.		6.98 E07	6.55 E07	6.143 E07

Table D VIII. Results ($V = 115{,}000$, $\rho_1 = 1.265.10^{-8}$, $\rho_0 = 10^{-9}$, $T_1 = 9500$, $T_2 = 5000$, $P = 1.1167.10^{-2}$)

	$L_1 = 1.0$	$L_1 = .95$	$L_1 = .90$	$L_1 = .85$
	$L_2 = 0.0$	$L_2 = .05$	$L_2 = .10$	$L_2 = .15$
T.T. Flux	1.12 E07	1.21 E07	1.29 E07	1.38 E07
L.L. Flux	1.09 E07	1.19 E07	1.28 E07	1.37 E07
C.C. Flux	3.28 E05	3.10 E05	2.92 E05	2.75 E05
HL-CC Flux		1.04 E07	1.00 E07	9.58 E06
T.T. Int.	1.96 E06	2.48 E06	2.60 E06	2.72 E06
L.L. Int.	2.29 E06	2.43 E06	2.56 E06	2.70 E06
C.C. Int.	5.26 E04	4.99 E04	4.72 E04	4.45 E04
HL-CC Int.		2.21 E06	2.13 E06	2.05 E06

Table D IX. Results ($V = 190{,}000$, $\rho_1 = 1.261.10^{-6}$, $\rho_0 = 10^{-7}$, $T_1 = 17, 957$, $T_2 = 5000$, $P = 3.0868$)

	$L_1 = .10.0$	$L_1 = 9.5$	$L_1 = 9.0$	$L_1 = 8.5$
	$L_2 = 0.0$	$L_2 = 0.5$	$L_2 = 1.0$	$L_2 = 1.5$
T.T. Flux	2.54 E12	8.45 E11	7.52 E11	7.09 E11
L.L. Flux	1.30 E12	8.10 E11	7.82 E11	7.61 E11
C.C. Flux	2.08 E12	1.52 E12	1.42 E12	1.35 E12
HL-CC Flux		8.77 E11	8.05 E11	7.54 E11
T.T. Int.	6.29 E11	2.61 E11	2.29 E11	2.12 E11
L.L. Int.	2.98 E11	2.07 E11	3.46 E11	3.25 E11
C.C. Int.	5.36 E11	3.75 E11	3.46 E11	3.25 E11
HL-CC Int.		1.89 E11	1.70 E11	1.55 E11

Table D X. Results (V = 190,000, $\rho_1 = 1.261.10^{-6}$, $\rho_0 = 10^{-7}$, $T_1 = 17{,}957$, $T_2 = 5{,}000$, P = 3.0868)

	$L_1 = 0.1$	$L_1 = .095$	$L_1 = .090$	$L_1 = .085$
	$L_2 = 0.0$	$L_2 = .005$	$L_2 = .010$	$L_2 = .015$
T.T. Flux	5.25 E11	4.71 E11	4.32 E11	4.01 E11
L.L. Flux	7.68 E10	7.40 E10	7.19 E10	6.98 E10
C.C. Flux	4.77 E11	4.32 E11	3.98 E11	3.70 E11
HL-CC Flux		6.49 E10	5.70 E10	5.09 E10
T.T. Int.	1.13 E11	1.07 E11	1.00 E11	9.35 E10
L.L. Int.	1.63 E10	1.60 E10	1.57 E10	1.53 E10
C.C. Int.	1.03 E11	9.59 E10	8.95 E10	8.35 E10
HL-CC Int.		1.49 E10	1.36 E10	1.25 E10

Table D XI. Results ($V = 190{,}000$, $\rho_1 = 1.261.10^{-6}$, $\rho_0 = 10^{-7}$, $T_1 = 17{,}957$, $T_2 = 7000$, $P = 3.0868$)

	$L_1 = 1.0$ $L_2 = 0.0$	$L_1 = .95$ $L_2 = .05$	$L_1 = .90$ $L_2 = .10$	$L_1 = .85$ $L_2 = .15$
T.T. Flux	1.24 E12	8.17 E11	7.28 E11	6.75 E11
L.L. Flux	3.38 E11	3.23 E11	3.11 E11	3.01 E11
C.C. Flux	1.14 E12	7.46 E11	6.71 E11	6.26 E11
HL-CC Flux		1.81 E11	1.53 E11	1.36 E11
T.T. Int.	3.49 E11	2.48 E11	2.20 E11	2.06 E11
L.L. Int.	7.51 E10	7.28 E10	7.08 E10	6.88 E10
C.C. Int.	3.30 E11	2.32 E11	2.06 E11	1.93 E11
HL-CC Int.		4.24 E10	3.39 E10	2.99 E10

Table D XII. Results ($V = 190{,}000$, $\rho_1 = 1.261.10^{-6}$, $\rho_0 = 10^{-7}$, $T_1 = 17{,}957$, $T_2 = 3000$, $P = 3.0868$)

	$L_1 = 1.0$	$L_1 = .95$	$L_1 = .90$	$L_1 = .85$
	$L_2 = 0.0$	$L_2 = .05$	$L_2 = .10$	$L_2 = .15$
T.T. Flux	1.24 E12	1.06 E12	1.03 E12	1.01 E12
L.L. Flux	3.38 E11	2.73 E11	2.62 E11	2.53 E11
C.C. Flux	1.14 E12	1.11 E12	1.09 E12	1.06 E12
HL-CC Flux		3.21 E11	3.05 E11	2.89 E11
T.T. Int.	3.49 E11	3.23 E11	3.16 E11	3.10 E11
L.L. Int.	7.51 E10	6.43 E10	6.15 E10	5.92 E10
C.C. Int.	3.30 E11	3.24 E11	3.19 E11	3.13 E11
HL-CC Int.		7.20 E10	6.88 E10	6.58 E10

Appendix E. Corrected Results

An error was detected in the computer program for the calculation of the position of the hydrogen edges. The position of the hydrogen edges was obtained in non-dimensional $h\nu/kt$ units instead of $h\nu$ units. Figure 22 shows the corrected plot of the spectral absorption coefficient of hydrogen. The position of Lyman edge in Figure 9 was at 8.7 ev, while it is at 13.4 ev in Figure 22.

The change in position of hydrogen edges effects the continuum absorption coefficient of hydrogen. Tables E I and E II show the correct results for the two cases at the conditions which are same as those of Tables D IX and D I, respectively. It is seen that the trends in the results do not change much but, the numerical values of flux and intensity change considerably. The continuum flux is reduced because the hydrogen edges are shifted to higher frequencies. Similar results will be expected for all the cases where the temperature of the hydrogen layer is above 11,605^{o}K. For the cases where the hydrogen layer temperature is less than 11,605^{o}K, the continuum flux will increase as compared to the previous results.

There is no change in the conclusions regarding the addition of carbon ablation layer. Figure 23 is the corrected plot for the Figure 17. There is not much of change in the shape of the curve, but, the values of flux at

Table E I. Corrected Results (V=190,000, ρ_1=1.261.10^{-6}, $\rho_0 = 10^{-7}$, T_1 = 17,957, T_2 = 5000, P=3.0868)

	L_1 = 10.0	L_1 = 9.5	L_1 = 9.0	L_1 = 8.5
	L_2 = 0.0	L_2 = 0.5	L_2 = 1.0	L_2 = 1.5
T.T. Flux	1.50 E12	4.44 E11	3.80 E11	3.46 E11
L.L. Flux	1.30 E12	8.08 E11	7.80 E11	7.59 E11
C.C. Flux	3.18 E11	1.70 E11	1.62 E11	1.53 E11
HL-CC Flux		8.77 E11	8.05 E11	7.54 E11
T.T. Int.	3.04 E11	1.14 E11	9.41 E10	8.28 E10
L.L. Int.	2.98 E11	2.07 E11	1.99 E11	1.92 E11
C.C. Int.	7.48 E10	2.93 E10	2.79 E10	2.64 E10
HL-CC Int.		1.89 E11	1.09 E11	1.55 E11

Table E II. Corrected Results ($V=190,000$, $\rho_1=1.086.10^{-5}$ $\rho_0=10^{-6}$, $T_1=21,380$, $T_2=5000$, $P=3.08.10^{1}$)

	$L_1 = 1.0$	$L_1 = 0.95$	$L_1 = 0.90$	$L_1=0.85$
	$L_2 = 0.0$	$L_2 = 0.05$	$L_2 = 0.10$	$L_2=0.15$
T.T. Flux	6.29 E12	1.86 E12	1.66 E12	1.52 E12
L.L. Flux	5.07 E12	3.07 E12	3.09 E12	2.95 E12
C.C. Flux	2.31 E12	1.48 E12	1.42 E12	1.35 E12
HL-CC Flux		3.61 E12	3.37 E12	3.16 E12
T.T. Int.	1.43 E12	5.26 E11	4.67 E11	4.26 E11
L.L. Int.	1.25 E12	8.47 E11	8.22 E11	8.04 E11
C.C. Int.	5.34 E11	2.83 E11	2.68 E11	2.54 E11
HL-CC Int.		8.62 E11	7.99 E11	7.45 E11

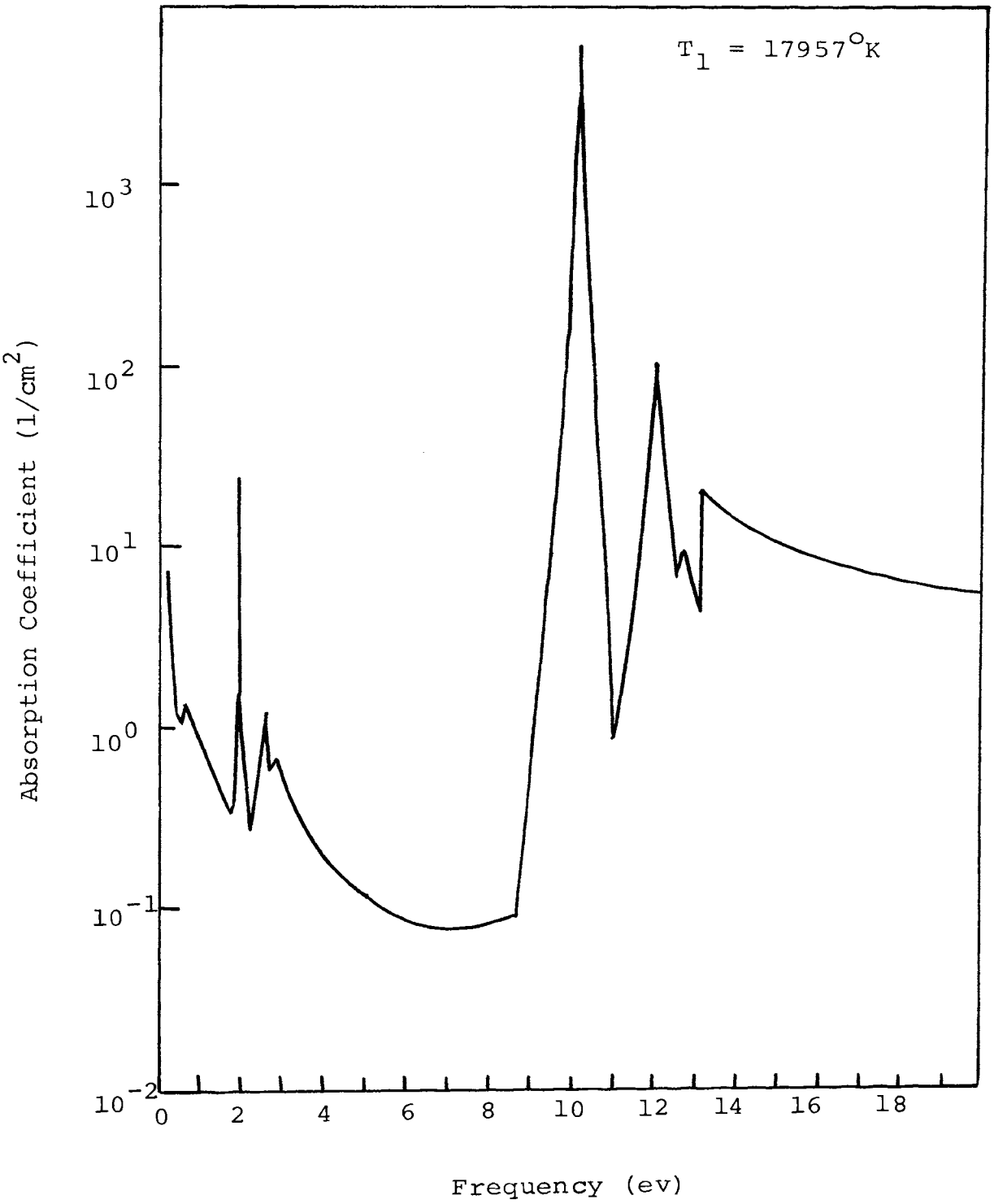

FIGURE 22. HYDROGEN ABSORPTION COEFFICIENT (corrected)

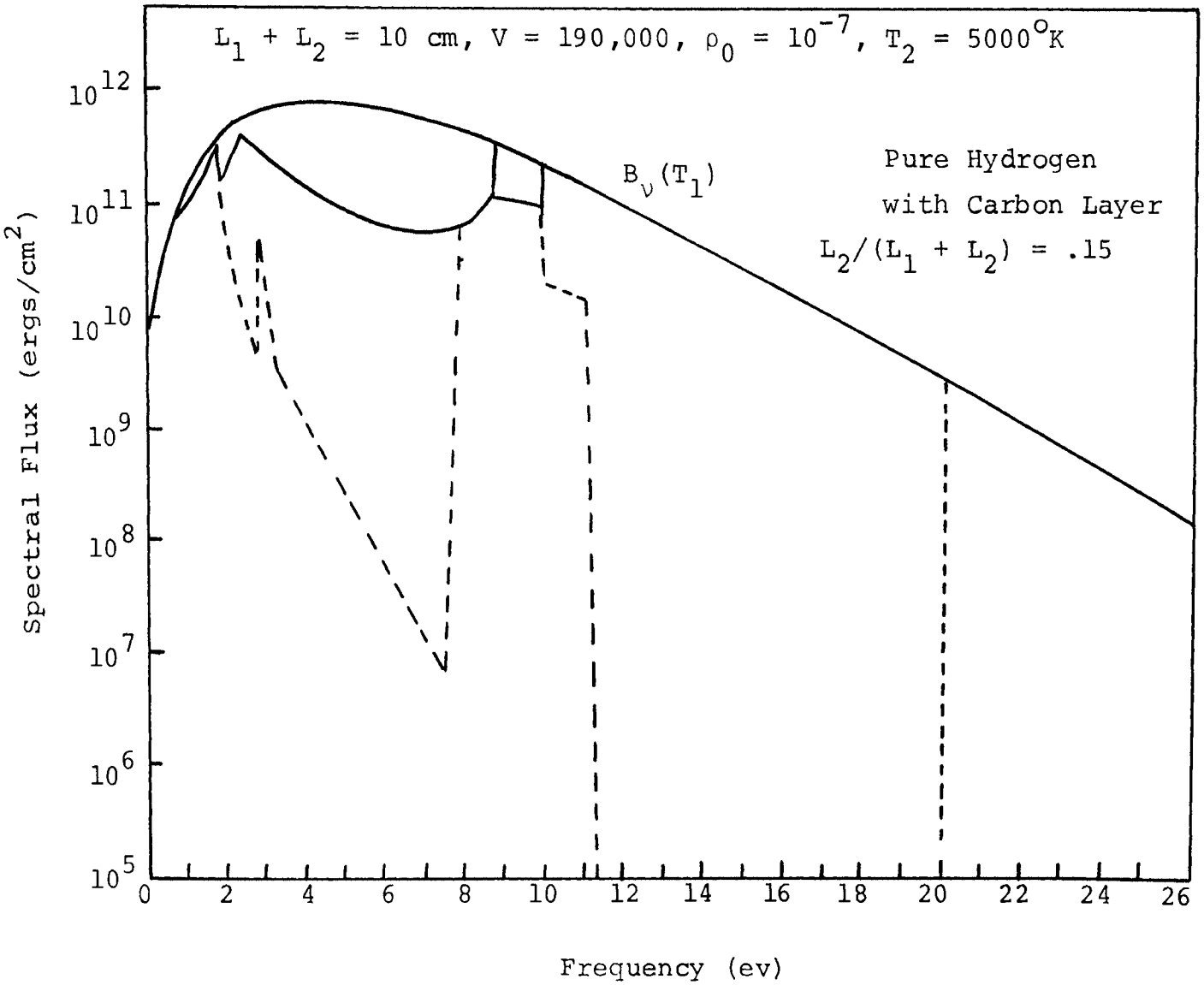

FIGURE 23. SPECTRAL FLUX DISTRIBUTION

various frequencies are changed. So there is no change in the conclusions obtained, but the numerically values of flux and intensity will be reduced for the cases where the hydrogen layer temperature is more than 11,605^{o}K. The positions of the hydrogen continuum edges were incorrectly calculated in the results shown in the body of the thesis. The position of Lyman edge which should be near 13.2 ev fluctuated in the previous results, as shown below:

Temperature ^{o}K	ρ, gm/cm^3	Lyman edge (ev)
21,380	1.086×10^{-5}	7.4
17,957	1.261×10^{-6}	8.7
15,272	1.452×10^{-7}	10.3
13,180	1.652×10^{-8}	12.0
13,395	9.22×10^{-6}	11.7
11,957	1.02×10^{-6}	13.1
10,669	1.142×10^{-7}	14.7
9,500	1.265×10^{-8}	16.5

The error in the flux and intensity was of the order of 50% in the two cases which were recalculated. In other cases it is likely to be less because cases recalculated involved the maximum change in the edge position. The error should be very small for the case where the Lyman edge was 13.1 (T = 11, 957 ^{o}K, $\rho_1 = 1.02 \times 10^{-6}$ gm/cm^3).

The computer program error only influenced the continuum calculations so that the previous L-L calculations are correct.

VIII. BIBLIOGRAPHY

1. Nelson, H.F., and Goulard, R., "Equilibrium Radiation from Isothermal Hydrogen-Helium Plasmas," Journal of Quantitative Spectroscopy and Radiative Transfer, Vol. 8, pp. 1351-1372, (1968).

2. Nelson, H.F., Private communication.

3. Aroeste, H., and Benton, W.C., "Emissivity of Hydrogen Atoms at High Temperatures," Journal of Applied Physics, Vol. 27, pp. 117, (1956).

4. Olfe, D.B., "Equilibrium Emissivity Calculations for a Hydrogen Plasma at Temperatures up to 10,000^{o}K," Journal of Quantitative Spectroscopy and Radiative Transfer, Vol. 1, pp. 104, (1961).

5. Biberman, L.M., Vorobev, K.S., and Norman, G.E., "Energy Emitted in Spectral Lines by a Plasma," Optics and Spectroscopy, Vol. 14, pp. 176, (1963).

6. Lasher, L.E., Wilson, K.H., and Greif, R., "Radiation From an Isothermal Hydrogen Plasma at Temperatures up to 40,000^{o}K," Journal of Quantitative Spectroscopy and Radiative Transfer, Vol. 7, pp. 305, (1967).

7. Griem, H.R., "Plasma Spectroscopy," McGraw-Hill,(1964).

8. Howe, J.T., and Scheaffer, Y.S., "Mass Addition in the Stagnation Region for Velocities up to 50,000 Feet per Second," NASA TR R-207, (1964).

9. Hoshizaki, L., and Lasher, L.E., "Convective and Radiative Heat Transfer to an Ablating Body," AIAA Journal, Vol. 6, pp. 1441-1449, (1968).

10. Chin, J.H., "Radiation Transport for Stagnation Flows Including Effects of Lines and Ablation Layer," AIAA Journal, Vol. 7, pp. 1310-1318, (1968).

11. Wilson, K.H., "Stagnation Point Analysis of Coupled Viscous Radiating Flow with Massive Blowing," LMSC, 687209, (1969).

12. Sparrow, E.M., and Cess, R.D., "Radiation Heat Transfer," Brooks/Cole Publishing Company, (1967).

13. Gilmore, F.R., "The Equilibrium Thermodynamic Properties of High Temperature Air," LMSC Palo Alto, California, (1967).

14. Fickett, W., and Cowan, R.D., "Values of Thermodynamic Functions to 12,000^{o}K for Several Substances," Journal of Chemical Physics, Vol. 23, pp. 1349-1350, (1955).

15. McBride, B.J., "Thermodynamic Properties to 6000^{o}K for 210 Substances," NASA SP-3001, (1963).

16. Zeldovich, Yu.B., and Raizer, Yu.P., "Physics of Shock Waves and Hydrodynamic Phenomena," Academic Press, (1966).

17. Biebermann, L.M., and Norman, G.E., "Recombination Radiation and Bremstrahlung of a Plasma," Journal of Quantitative Spectroscopy and Radiative Transfer, Vol. 3, pp. 221-245, (1963).

18. Wilson, K.H., and Nicolet, W.E., "Spectral Absorption Coefficients of Carbon, Nitrogen, and Oxygen Atoms," Journal of Quantitative Spectroscopy and Radiative Transfer, Vol. 7, pp. 891, (1967).

19. Weise, W.L., Smith, M.W., and Glennon, B.M., "Atomic Transition Probabilities-Hydrogen Through Neon," NSRDS-NBS 4, (1966).

20. Krascella, N.L., "Tables of the Composition, Opacity, and Thermodynamic Properties of Hydrogen at High Temperatures," NASA SP-3005, (1963).

21. Bogers, A. III., "The Emission Spectra of H_2^+," Astro-Physical Journal, Vol. 129, PD. 43, (1959).

22. Darwin, H.W., and Felenbok, P., "Data for Plasmas in Local Thermodynamic Equilibrium," Gauther-Villars, Paris, (1965).

23. Rosenbaum, B.M., and Levitt, H.L., "Thermodynamic Properties of Hydrogen from Room Temperature to 100,000^{o}K," NASA TN D-1107, (1962).

24. Patch, R.W., and McBride, B.J., Partition Functions and Thermodynamic Properties to High Temperatures for H_3T and H_2^+," NASA TN D-4523, (1968).

25. Patch, R.W., "Absorption Coefficients for Hydrogen," Journal of Quantitative Spectroscopy and Radiative Transfer, Vol. 9, pp. 63-87, (1969).

IX. VITA

Birbal Singh was born on July 10, 1943 in district Jhunjhunu, Rajasthan, India. He received his secondary school education in Jhunjhunu, India. He has received his college education from Podar College, Nawalgarh, India. He received a Bachelor of Technology degree in Mechanical Engineering from the Indian Institute of Technology, Bombay, in January, 1965.

He worked as an Associate Lecturer in the Mechanical Engineering Department, Indian Institute of Technology, Bombay, from February 1965 to August 1966. He joined the Birla Institute of Technology and Science, Pilani, India, as a Lecturer in Mechanical Engineering Departmetn in September 1966, and worked up to July 1969.

He has been enrolled in the Graduate School of the University of Missouri-Rolla since September 1969.